MacroH2A histone variants maintain nuclear organization and heterochromatin architecture

Julien Douet[1,2], David Corujo[1,2,*], Roberto Malinverni[1,2,*], Justine Renauld[3], Viola Sansoni[4], Melanija Posavec Marjanović[1], Neus Cantariño[1], Vanesa Valero[1,2], Fabien Mongelard[5], Philippe Bouvet[5], Axel Imhof[4], Marc Thiry[3] and Marcus Buschbeck[1,2,6]

[1]Josep Carreras Leukaemia Research Institute (IJC), Campus ICO – Germans Trias i Pujol, Campus Can Ruti, 08916 Badalona, Spain.
[2]Institute of Predictive and Personalized Medicine of Cancer (IMPPC), Campus Can Ruti, 08916 Badalona, Spain.
[3]Cell and tissue biology unit, GIGA-Neurosciences, University of Liege, C.H.U. Sart Tilman, Liege 4000, Belgium.
[4]BioMedical Center and Center for Integrated Protein Sciences Munich, Ludwig-Maximilians-University of Munich, Großhaderner Straße 9, 82152 Planegg-Martinsried, Germany.
[5]Université de Lyon, Ecole normale Supérieure de Lyon, Centre de Recherche en Cancérologie de Lyon, Cancer Cell Plasticity Department, UMR INSERM 1052 CNRS5286, Centre Léon Bérard, Lyon, France
[6]Corresponding author. IJC, Campus Can Ruti, Ctra de Can Ruti, IMPPC building, Cami de les Escoles w/o number; 08916 Badalona, Spain. Telephone: 0034-934651472. Fax: 0034-934651472. E-mail: mbuschbeck@carrerasresearch.org

*These authors have contributed equally.

Summary statement: MacroH2A links nucleosome composition to higher order chromatin architecture, in part by mediating the interaction of heterochromatin repeats to the nuclear lamina.

Journal of Cell Science • Advance article

JCS Advance Online Article. Posted on 10 March 2017

ABSTRACT

Genetic loss-of-function studies in development, cancer and somatic cell reprogramming have suggested that the group of macroH2A histone variants might function through stabilizing the differentiated state by a yet unknown mechanism. Here, we present results demonstrating that macroH2A variants have a major function in maintaining nuclear organization and heterochromatin architecture. Specifically, we find that a substantial amount of macroH2A is associated with heterochromatic repeat sequences. We further identify macroH2A on sites of interstitial heterochromatin decorated by H3K9me3. Loss of macroH2A leads to major defects in nuclear organization including reduced nuclear circularity, disruption of nucleoli and a global loss of dense heterochromatin. Domains formed by repeat sequences when depleted of macroH2A are disorganized, expanded and fragmented and mildly re-expressed. On the molecular level we find that macroH2A is required for the interaction of repeat sequences with the nucleostructural protein Lamin B1. Taken together our results argue that a major function of macroH2A histone variants is to link nucleosome composition to higher order chromatin architecture.

INTRODUCTION

A large number of loss of function studies support a physiological role for macroH2A histone variants in the establishment and maintenance of differentiated epigenomes. MacroH2A proteins promote differentiation of embryonic and adult stem cells (Creppe et al., 2012a), are important for proper embryonic development of Zebrafish (Buschbeck et al., 2009) and form an epigenetic barrier to somatic cell reprogramming (Barrero et al., 2013a; Gaspar-Maia et al., 2013; Pasque et al., 2011; Pasque et al., 2013). In the context of cancer, the bulk literature positions macroH2A proteins as *bona fide* tumor suppressors (reviewed in Cantariño et al., 2013). In melanoma macroH2A expression is lost in advanced stages and re-expression of macroH2A proteins suppresses metastatic potential (Kapoor et al., 2010). Suppression of macroH2A1 enhanced the cancer stem cell-like properties in bladder cancer (Park et al., 2015) and lead to a massive expansion of undifferentiated carcinoma-like tissue in teratomas grown from xenografted mouse embryonic stem cells (Creppe et al., 2012a).

MacroH2A has a still unexplained ambiguous role in transcriptional regulation. While macroH2A's genomic distribution anti-correlates with transcriptional activity (Changolkar and Pehrson, 2006; Changolkar et al., 2010; Gamble et al., 2010), it is in some cases required for signal-induced gene activation (discussed in Creppe et al., 2012b). The repressive function of macroH2A proteins has been primarily associated with cancer. In both melanoma and breast cancer macroH2A was for instance shown to exert its tumor suppressive function through repression of the cell cycle promoting gene *CDK8* (Kapoor et al., 2010; Xu et al., 2015). Lavigne and colleagues provided results suggesting that rather than being a transcriptional regulator macroH2A proteins stabilize expression states thus providing robustness and reducing noise (Lavigne et al., 2015).

Both macroH2A1 and macroH2A2 co-occupy promoters of developmental genes that are bound by Polycomb repressive complexes (Buschbeck et al., 2009) and large macroH2A-bound regions overlap with the Polycomb mark H3K27me3 (Gamble et al., 2010). Polycomb-bound and H3K27me3-marked regions are frequently referred to as facultative heterochromatin that has been defined as a transiently condensed and transcriptionally silent type of chromatin permissive to transcriptional activation in response to environmental and differentiation signals (Trojer and Reinberg, 2007).

In contrast, constitutive heterochromatin is characterized by its stable repressive nature. The histone mark H3K9me3 plays an important role in its establishment and maintenance (Maison and Almouzni, 2004). H3K9me3 is enriched in gene-poor genomic regions containing repetitive elements and is believed to largely encompass the same genomic locations in different cell types. As such, constitutive heterochromatin is considered to be a more static structure than Polycomb-marked chromatin. The DNA sequences contained in constitutive heterochromatin include telomeric and pericentromeric satellite repeats, transposable elements such as long interspersed

DNA elements (LINEs) and long terminal repeats (Peters et al., 2003; Rice et al., 2003). An important function of constitutive heterochromatin is to prevent genomic instability and ensure stable replication of the genome by maintaining transposons and simple DNA repeats transcriptionally silent (Bouzinba-Segard et al., 2006; Peters et al., 2003; Taddei et al., 2001).

One of the most conserved characteristics of genome organization is the accumulation of heterochromatin close to the nuclear lamina, constituted in mammals by a meshwork of 4 lamin proteins and a number of transmembrane proteins (reviewed in Amendola and van Steensel, 2014; Gruenbaum and Medalia, 2015). Three genes *LMNA*, *LMNB1* and *LMNB2* encode the four major mammalian lamins: the splice variants Lamin A and C, Lamin B1 and Lamin B2. Mapping techniques such as DamID have demonstrated that lamins are enriched over domains ranging from 10 kb to 10 Mb in size that were termed lamin-associated domains (LADs; Guelen et al., 2008). In particular those LADs that have high cell-to-cell consistency are inversely linked with gene activity and associated with H3K9me3 (Kind et al., 2015). Importantly, in both *C. Elegans* and human cells H3K9-specific methylases and resulting H3K9me2/3 levels were required for the tethering of genomic loci to the nuclear lamina (Bian et al., 2013; Kind et al., 2013; Towbin et al., 2012). It is still unclear to which extent other marks enriched in LADs such as H3K27me3 also contribute to tethering (Guelen et al., 2008; Harr et al., 2015).

While Lamin B proteins are primarily localized at the periphery interacting with heterochromatin, a substantial fraction of Lamin A/C is also found in the nucleoplasm and interacts with euchromatic regions (Gesson et al., 2016). In the nucleoplasm Lamin A/C further interacts with the surface of Polycomb-marked heterochromatin foci (Cesarini et al., 2015). In addition to the nuclear lamina, the nucleolus is the other nuclear structure with a major influence in genome organization and surrounded by a shell of constitutive heterochromatin (Németh et al., 2010). Besides ribosomal DNA, the nucleolus-associated sequences are highly similar to LADs suggesting that the nuclear lamina and the nucleolus are two alternative locations for similar types of repressive genomic domains (Németh et al., 2010; van Koningsbruggen et al., 2010). Noteworthy, Lamin B1 but not Lamin A/C is required for the preservation of nucleolar structure (Martin et al., 2009).

The nuclear organization and in particular the capacity to anchor part of the genome at the nuclear periphery is emerging as an important parameter for differentiation and development. This is best demonstrated in the context of myogenic differentiation which is impaired after inactivation of proteins mediating the perinuclear tethering of genomic regions (Gonzalez-Sandoval et al., 2015; Robson et al., 2016). The large majority of reported loss-of-function phenotypes support the idea that macroH2A proteins function through stabilizing the differentiated state by a yet unknown mechanism. Here, we have tested the hypothesis that macroH2A proteins function through

regulating nuclear organization. Using a combination of cytological and biochemical techniques, we unveil a major role of macroH2As in the maintenance of nuclear organization and heterochromatin architecture. Specifically, we report that macroH2A1 and macroH2A2 are bound to heterochromatic repeats and contribute to the tethering of these repeats to the nuclear lamina.

RESULTS

MacroH2A is essential for maintaining nuclear organization and nucleolar integrity.

To get a global view of nuclear organization and a possible influence of macroH2A we have analyzed cells after depletion of both macroH2A1 and macroH2A2. We have selected the well-characterized human male HepG2 cell line as model system. HepG2 cells express both macroH2A1 and macroH2A2 isoforms (Figure 1A) The knockdown of both macroH2A1 and macroH2A2 using stably integrated shRNA cassettes was highly efficient (Figure 1A and B). As shown in Figure 1C, depletion of macroH2A proteins had a major effect on the nuclear organization and shape. Nuclei in control cells show well-shaped nucleoli and regions of dense heterochromatin staining in the nucleoplasm and at nuclear and nucleolar periphery. Knockdown of macroH2A proteins led to the global loss of dense heterochromatin. This loss of dense heterochromatin was most pronounced at the classic sites of heterochromatin accumulation, the surface of the nucleolus and the nuclear periphery but could also be observed in the nucleoplasm (Figure 1C-D). This effect had a very high penetration in the cell population and when analyzing more than 100 cells we could not identify a single knockdown cell with intact dense heterochromatin (Figure 1E). In knockdown cells, nucleoli were expanded and had a reticulated appearance with several small fibrillar centers (Figure 1D). Such structural changes in nucleolar organization are indicative of increased transcriptional activity of rDNA, which we previously reported in macroH2A-depleted cells (Cong et al., 2013). We have confirmed the nucleolar expansion by immunofluorescence using nucleophosmin as marker to stain nucleoli (Figure 1F). Conversely, macroH2A1 staining was found in the entire nucleus except in the nucleoli (Figure 1B). Quantification by automated area measurements of 2D projections revealed both the nucleus and nucleolus are increased in size in macroH2A-deficient cells (Figure 1G and H). The increase in nucleolar size remained significant after normalizing for the nuclear expansion (Figure 1H). The electron microscopic image already indicated the appearance of nuclei with irregular shape (Figure 1C). Analysis of confocal images showed that the proportion of nuclei displaying anomalies such as the formation of bud-like structures or cavities was significantly increased in the absence of macroH2A proteins (Figure 1I). Taken together these results make a compelling case for an

important role of macroH2A proteins in maintaining nuclear organization including nucleolar and heterochromatic structures.

A substantial fraction of macroH2A-bound chromatin coincides with H3K9me3.

To gain a better understanding of the relation between macroH2A and heterochromatic features, we analyzed both the DNA sequence and the histone H3 modifications of macroH2A-bound chromatin. We have used specific, non-crossreacting antibodies (Supplementary Figure S1) to determine the distribution of macroH2A1 and macroH2A2 on the linear genome by ChIP-seq. The antibody used for macroH2A1 has been generated against the extranucleosomal domain and does not distinguish between the different splice variants of macroH2A1 (Pehrson et al., 1997). The analysis of our ChIP-seq data confirmed several of the characteristics that were previously described for macroH2A proteins in other cell types suggesting that our data is of high quality (Supplemental Figure S2A and B). These features are a significant enrichment over large domains and to a large extent to intergenic domains (Gamble et al., 2010), an overall high similarity between macroH2A1 and macroH2A2 (Gaspar-Maia et al., 2013; Pehrson et al., 2014), and an anti-correlation with transcribed regions (Changolkar and Pehrson, 2006; Changolkar et al., 2010; Gamble et al., 2010). To compare the association of macroH2A proteins with the two major marks of constitutive and facultative heterochromatin, H3K9me3 and H3K27me3, respectively, we took advantage of available HepG2 ChIP-seq data of these marks generated by the ENCODE project (ENCODE Consortium, 2012). Given the high similarity between macroH2A1 and macroH2A2 (see example given in Supplemental Figure S2A), we have focused on one of the two proteins and found that 50% all macroH2A2-bound peaks were overlapping with H3K27me3 peaks and only around 10% with H3K9me3 (Figure 2A). These results were in line with previous epigenomic analyses concluding that the facultative heterochromatin mark H3K27me3 is the predominant histone H3 tail modification overlapping with macroH2A-bound regions (Chen et al., 2014; Gamble et al., 2010; Gaspar-Maia et al., 2013).

The biochemical analysis of the tail modifications of histone H3 associated with macroH2A, however, presented a different picture. This analysis indicated that the amount of K9me3-modified histone H3 associated with macroH2A1.2 is in a similar range as the amount of associated H3K27me3 (Figure 2B). Specifically, we have used HepG2 cells expressing epitope-tagged macroH2A1.2 on the same level as the endogenous protein and compared the relative amount of histone H3 modifications on isolated macroH2A1.2-containing nucleosomes with equimolar standards of pure modified histone H3 proteins generated by chemical ligation (Bartke et al., 2010). Similar results were obtained using HEK293T cells (Supplemental Figure S2C). Taken together these results suggested that ChIP-seq analyses underestimate the association between macroH2A and constitutive heterochromatin.

To better understand where in the genome macroH2A and H3K9me3 co-occur, we took a closer look at the 10% fraction of macroH2A2 peaks that overlap with H3K9me3 while being devoid of H3K27me3 (Figure 2A and C). These 1180 peaks mark 1-5 kb regions and are often found isolated in euchromatic or Polycomb-marked environments and thus correspond to regions of interstitial heterochromatin (Figure 2D). In the genome enrichment plots, many of these interstitial heterochromatic regions are easily seen as sharp peak-like enrichments of H3K9me3 coinciding with macroH2A1 and macroH2A2 (Figure 2D). We confirmed the specific enrichment of macroH2A1, macroH2A2 and H3K9me3 on these peaks in independent ChIP experiments performed with control cells and macroH2A-deficient cells (Figure 2E and Supplemental Figure S2D). The level of enrichment of macroH2A2 on these interstitial peaks tended to be higher than on other macroH2A-bound sites such as the macroH2A2 target gene *LAMA5* (Figure 2E).

These results highlight the presence of macroH2A on isolated regions of interstitial heterochromatin. However, the number and size of these regions do not appear sufficient to provide an explanation for the substantial amount of H3K9me3 that we found associated with the immunoprecipitated macroH2A.

MacroH2A is bound on constitutive heterochromatin repeats.

As a hallmark of constitutive heterochromatin H3K9me3 is tightly associated with repeat sequences. Repeatmasker (Smit et al.) classifies the subfraction of repeat elements that have been annotated so far. We have used the permutation test-based R package regioneR (Gel et al., 2015) to assess if macroH2A peaks are significantly associated with any of class of these repetitive elements. We found that peaks of both macroH2A proteins were positively associated with several types of repeats (Figure 3A). The number of repeat classes that positively associated further increased when analyzing the fraction of peaks shared with H3K9me3 (Figure 3A).

Given the association of macroH2A with annotated repeats, we next tested whether macroH2A also binds classic heterochromatic repeats that are still largely excluded from the current genome built. These included the pericentromeric *SAT2* repeat, the centromeric alpha-satellite repeat, *45S* and *5S* ribosomal DNA and *DXZ4*, a repeat located on the X chromosome and known to be H3K9me3 marked in male cells (Chadwick, 2008). As shown in Figure 3B, we found a significant enrichment of macroH2A2 proteins on all these repeats that was in a similar range as on two known, Polycomb-marked target genes of the HOX family (Buschbeck et al., 2009). Similar results were obtained for macroH2A1 (Supplemental Figure S3A). Knockdown of both macroH2A did neither affect the level of H3K9me3 neither on repeats (Figure 3C and Supplemental Figure S3B) nor on interstitial heterochromatin peaks (Figure 2E). Comparable results were obtained when analyzing macroH2A1 in mouse embryonic fibroblasts from macroH2A1 KO animals and control mice; macroH2A1 was enriched on Line-L1, ribosomal DNA, minor and major satellite repeats and its loss did not affect H3K9me3 levels on any of these repeats (Supplemental Figure S3C and D).

Taken together these results demonstrate that macroH2A histone variants are enriched on repeats that constitute the core of constitutive heterochromatin. The fact that many of these repeat sequences are not annotated provides a plausible explanation for the underestimation of the overlap between macroH2A and H3K9me3 by ChIP-seq.

The integrity of heterochromatic repeat architecture depends on macroH2A.

Next, in order to determine what function macroH2A could exert on these repeats, we decided to take a closer look at the organization of two macroH2A-bound repeats, *45S* ribosomal DNA (rDNA) and *SAT2*. Approximately 300 copies of ribosomal *45S* rDNA repeats are distributed over five clusters in the human genome (reviewed in Diesch et al., 2014). Fluorescence *in situ* hybridization of *45S* rDNA showed a disorganization of foci in macroH2A knockdown cells (Figure 4A, top panel). Analysis of these images showed that while control cells have an average of 4,2 *rDNA* foci per nucleus, macroH2A knockdown cells had a significant increase to 7,4 foci (Figure 4A, top right panel). Similarly, the pericentromeric *SAT2* repeat from chromosome 1 showed a significant expansion of the FISH signal (Fig. 4A, middle panel). Next, we analyzed nuclear H3K9me3 staining as proxy for all heterochromatic areas and observed a global diffusion of the signal (Figure 4A, bottom panel). This can be quantified as a reduction in areas with signal above a determined threshold (Figure 4A, bottom right panel). In contrast to human cells, heterochromatin can be easily observed in mouse cells as a number of dense structures called chromocenters that are strongly stained by DAPI. Mouse embryonic stem cells predominantly express macroH2A1.2, which can be efficiently suppressed by a validated small hairpin RNA (Creppe et al., 2012a). When grown in the presence of serum chromocenters are present in mouse embryonic stem cells but significantly reduced in size when macroH2A1 was depleted (Supplemental Figure S4A and B). Next, we wished to test whether the observed deregulation of heterochromatin architecture would compromise the silencing of repeats. As shown in Figure 4B, we used RT-qPCR to measure the transcripts of a panel of repeats and observed an increase of RNA transcripts for all of them. The impact on transcript level varied and ranged from a subtle increase in *5S* ribosomal RNA to a 3-fold increase of *DXZ4* transcripts. These results suggest that macroH2A proteins have a major contribution to the three-dimensional architecture of repeats and a minor contribution to their transcriptional repression.

Next, we asked how macroH2A could mediate its function in heterochromatin architecture. Specifically, we wondered whether loss of macroH2A would affect the compaction and condensation of heterochromatin on the level of the DNA fiber. For this we have used two complementary methods to measure the openness and nucleosome density. First, we have used an formaldehyde-assisted isolation of regulatory elements (FAIRE) assay (Simon et al., 2012) to assess a possible change in openness. While we were able to clearly distinguish between two well-characterized open and closed gene loci, we did not detect any difference on repeats in the

absence or presence of macroH2A (Figure 4C). Second, the analysis of histone H3 occupancy similarly demonstrated that the nucleosome density is equal in control and macroH2A-depleted cell (Figure 4D). Taken together, these results suggest that the observed expansion of territories occupied by repeats in the nuclear space is not a consequence of decondensation of the fiber but rather occurring on the level of higher order chromatin structures.

MacroH2A is required for the attachment of repeats to Lamin B1.

The nuclear periphery is the region with the highest density of heterochromatin and here its loss after macroH2A depletion was particular striking (Figure 1D). Thus, we wondered whether macroH2A could be involved in mediating the interaction of heterochromatic repeats with the nuclear lamina. Interestingly, we found that knockdown of the consistently lamina-associated protein Lamin B1 resulted in an expansion of the *SAT2* repeat that was reminiscent of the phenotype caused by macroH2A depletion (Supplemental Figure S4C-E). Thus, we decided to test for a potential interaction between macroH2A-containing chromatin fibers with Lamin B1. We have used *in situ* proximity ligation assay (PLA), which is based on the proximity of two antibody-binding events and can detect interactions in a distance of up to 40 nm. As chromatin fibers are expected to be between 10 nm and 30 nm in size, PLA is useful and has previously been used for the study of interactions between a histone modification and nucleosolic lamins (Cesarini et al., 2015). As shown in Figure 5A, we were able to detect an interactions between Lamin B1 and both macroH2A1 and macroH2A2. The number and location of detected interactions between macroH2A proteins and Lamin B1 was similar to the interactions between individual Lamin B1 proteins detected with two different antibodies (Supplemental Figure 6A and B). The specificity of the PLA signal is shown by the significant reduction in the number of signals in macroH2A depleted cells (Figure 5B). Using the same approach we found that the interaction between macroH2A1 and H3K9me3 was primarily detected at the nuclear periphery and thus in close proximity to the lamina (Figure 5C).

As LADs are to a large extent consistent between cell types (Meuleman et al., 2013), we mapped the enrichment of macroH2A reads from our ChIP-seq experiment in HepG2 cells across borders of LADs that were previously mapped in human IMR90 fibroblasts (Shah et al., 2013). As shown in Figure 5C, both macroH2A1 and macroH2A2 were enriched on LADs compared to neighbouring regions. The mapping of HepG2 ChIP-seq data from ENCODE confirmed the enrichment of H3K9me3 and the depletion of the transcription-associated mark H3K36me3 and RNA polymerase II on LADs (Figure 5D).

Having confirmed the interaction of macroH2A with Lamin B1 in HepG2 cells, we addressed the key question whether macroH2A would be required to mediate the interaction of repeat DNA with Lamin B1. For this, we performed ChIP experiments with a Lamin B1 antibody in control and

macroH2A-depleted cells. We found that Lamin B1 was significantly enriched on all repeats and that this enrichment was lost in macroH2A-depleted cells (Figure 6A) while overall levels and localization of Lamin B1 was unaffected (Figure 6B and C). To validate the finding on a more general level, we repeated the experiment with a different cell type from a different species and repressed the expression of macroH2A with a different hairpin vector. Analogous to the experiment in HepG2 cells, we observed that the highly efficient depletion of macroH2A1 in mouse embryonic stem cells did not affect the protein level of Lamin B1 (Figure 6D) but completely abolished its interaction with the tested repeats (Figure 6E). Finally, we have again used PLA to measure the interaction between H3K9me3 and Lamin B1 in HepG2 cells. As expected the interaction between H3K9me3 and Lamin B1 was detected at the nuclear periphery (Figure 6F). In further support of the ChIP experiments, this interaction was reduced in macroH2A-depleted cells (Figure 6F and G).

Taken together our results identify a major function for macroH2A in nuclear organization. This function includes the maintenance of heterochromatin architecture which macroH2A mediates at least in part by promoting the interaction of H3K9me3-marked repeats with Lamin B1.

DISCUSSION

In this study we provide compelling evidence for an important role for macroH2A histone variants in global nuclear organization. We have focused on the substantial – but until now underestimated – association of macroH2A with H3K9me3-marked heterochromatin. This includes well-known heterochromatin repeats such as pericentromeric satellites but also few kilobase small regions of interstitial heterochromatin found embedded in other chromatin environments. We find that macroH2A proteins are required for maintaining proper heterochromatin architecture, at least in part by mediating the interaction of these DNA elements with the nuclear lamina protein Lamin B1. Here we discuss the molecular and physiological implications of these findings.

MacroH2A is required for heterochromatin architecture

The loss of macroH2A proteins results in major changes in the three-dimensional organization of constitutive heterochromatin in the nuclear space. Domains occupied by specific repeat sequences were disorganized, partially decondensed and fragmented, an effect that correlated with a loss of Lamin B1 binding. Wen and co-workers have reported an enrichment of macroH2A1 in biochemical purifications of Lamin B1 (Fu et al., 2015). Extending on this finding we were able to show that this interaction occurs at the nuclear periphery and that macroH2A is required for the binding of Lamin B1 to H3K9me3-marked repeats. While previous studies in *C. Elegans* and human cells have demonstrated a role for readers and writers of H3K9 methylation in mediating the tethering of repeats to the nuclear lamina (Bian et al., 2013; Gonzalez-Sandoval et al., 2015; Kind et al., 2013; Towbin et al., 2012), our results now add macroH2A as a novel player. MacroH2A might either provide an additional interaction surface or stabilize the function of other factors. In particular, it is presently not clear whether the interaction between macroH2A and Lamin B1 is direct or indirect.

Importantly, we find that the influence of macroH2A loss on heterochromatin architecture was not restricted to heterochromatin proximal to the nuclear lamina but rather globally occurring throughout the nucleus including in the nucleosol and on the surface of nucleoli. This suggests that macroH2A proteins contribute also by Lamin B1-independent mechanism to heterochromatin architecture. A study in *Arabidopsis* has provided an important clue to how this could occur. *Arabidopsis* lacks macroH2A proteins but contains H2AW histone variants that resemble macroH2A variants without the macro domain. H2AW variants were shown to contribute to heterochromatin condensation in the nucleosol by mediating fiber-fiber interactions (Yelagandula et al., 2014). The Luger lab has previously shown that the linker domain of macroH2A1 has a similar condensation capacity *in vitro* (Muthurajan et al., 2011). Thus, it is conceivable that macroH2A might exert its function in heterochromatin architecture by mediating fiber-fiber interactions as well as an interaction with Lamin B1 at the nuclear periphery. Future work will need to dissect the individual contributions of these two mechanisms and to assess their possible

interdependence.

It is interesting to point out that the hypothetical existence of two parallel mechanisms is able to explain the large-scale re-organization of heterochromatin observed during senescence. Senescence is characterized by a progressive loss of Lamin B1 proteins (Freund et al., 2012; Shah et al., 2013) and the accumulation of dense macroH2A-containing heterochromatin foci in the nucleosol (Zhang et al., 2005). This could reflect a loss of macroH2A-Lamin B1 mediated tethering but persistent macroH2A-dependent fiber-fiber interactions.

In conclusion, taking our and Wen's results (Fu et al., 2015) together, they make a strong case for a general function of macroH2A proteins in heterochromatin architecture that is conserved from mouse to man, likely across all macroH2A-containing species. Since repetitive DNA constitutes about 60–70 % of the mammalian genome (Padeken et al., 2015), it is fair to say that the organization of these repeats in proper heterochromatin is a major function of macroH2A proteins.

MacroH2A is essential to maintain nuclear integrity

Apart from the reorganization of heterochromatic domains, we describe here a strong nuclear phenotype with a significantly increased proportion of irregular and larger nuclei in macroH2A-depleted cells. In addition, the nucleolar compartment displayed a general expansion and a severe disorganization including a loss of nuclei-associated heterochromatin. Although nuclear lamina and the nucleolar periphery are spatially and structurally distinct, they represent a similar environment for chromatin containing mostly the same heterochromatic repeat sequences (Németh et al., 2010; van Koningsbruggen et al., 2010). Indeed, the same locus located at the nuclear periphery can be found associated to the nucleolus of the daughter cells after cell division (Kind et al., 2013). It is interesting to point out that nucleoli were found to undergo major restructuration after Lamin B1 depletion (Martin et al., 2009) suggesting a link between both compartments.

It is conceivable that the changes in nuclear shape and nucleolar organization are caused by macroH2A-dependent changes in heterochromatin structure. As such our results further strengthen the idea that the nuclear shape does not only delimit the organization of chromatin but that also *vice versa*, the chromatin structure is determining the nuclear shape.

The fact that macroH2A can be also found in other chromatin environments provokes the intriguing speculation that the role of macroH2A in contributing to higher order chromatin structures might not be limited to constitutive heterochromatin but much more global. For instance, both epigenomic as well as imaging studies have pointed out that an important fraction of macroH2A is associated with Polycomb-marked chromatin (Buschbeck et al., 2009; Chadwick and Willard, 2004; Gamble et al., 2010). Ongoing work in our lab is addressing the question whether macroH2A plays a role in the three-dimensional organization of Polycomb domains.

The link between nuclear architecture and cell fate

Loss-of-function studies in development, cancer and somatic cell reprogramming have allowed the conclusion that macroH2A proteins contribute to maintaining the differentiated state of a cell by a yet unknown mechanism (reviewed in Posavec et al., 2013). Here, we show that macroH2A is required for the establishment and/or the maintenance of heterochromatin. The observed partial de-repression of some of these sequences in macroH2A-depleted cells is possibly secondary to changes in higher order chromatin architecture including loss of perinuclear tethering. An elegant study by Gasser and co-workers has demonstrated that in *Caenorhabditis elegans* tethering is essential for maintaining a developmentally induced cell fate (Gonzalez-Sandoval et al., 2015). Additionally, Robson and colleagues could show that a set of nuclear envelope transmembrane proteins was implicated in the relocalization and the transcriptional regulation of genes implicated in myogenic differentiation (Robson et al., 2016).

Conversely to its function in differentiation, macroH2A is a major barrier to the de-differentiation occurring during somatic cell reprogramming (Barrero et al., 2013b; Gaspar-Maia et al., 2013; Pasque et al., 2013; Pasque et al., 2011). Successful reprogramming requires the removal of somatic repressive marks to reach a chromatin state almost devoid of heterochromatin, and thus the dissolution of large heterochromatic domains represent a major obstacle (Soufi et al., 2012; Sridharan et al., 2013). Hence, the here reported stabilization of heterochromatin by macroH2A provides a possible explanation for its barrier function in somatic reprogramming.

Future work will need to address the question whether the changes in chromatin structure favor cancer by increasing the epigenetic plasticity or whether specific gene deregulation events drive cancer as suggested for the upregulation of the oncogene *CDK8* in macroH2A-deficient melanoma (Kapoor et al., 2010). Further it will be interesting to dissect whether relevant changes in cancer gene expression are a bystander effect of the massive genome re-organization caused by loss of macroH2A. It is plausible that the stabilization of structures is stabilizing gene expression programs and that in the context of repression some activating signals will overcome repression in the absence but not presence of macroH2A. In support of this idea it was shown that a combination of the gene activating anti-cancer drugs azacitidine and trichostatin were able to reactivate a repressed transgene on the inactive X chromosome only after depletion of macroH2A (Hernández-Muñoz et al., 2005).

In conclusion, macroH2A has a major function in chromatin architecture that we have studied on constitutive heterochromatin but that might not be limited to it. The stabilization of heterochromatin architecture and possibly other chromatin structures has great potential to provide a molecular explanation for its functions in development, cancer and somatic cell reprogramming. We would like to suggest that macroH2A should be considered as a global stabilizer of the genome and that its role in gene expression is likely to be secondary to its role in higher order chromatin

architecture.

MATERIAL AND METHODS

Cell Culture and gene transduction

The human male heptoblastoma cell line HepG2 and HEK293T cells were obtained from ATCC, authenticated and cultured in Dulbecco's modified Eagle medium (DMEM, Gibco) containing penicillin-streptomycin, 10% fetal bovine serum (FBS) and 2mM L-glutamine at 37°C in 5% CO2. For the culture of mouse embryonic fibroblasts (MEFs) the medium was further supplemented with 0.1 mM β-mercaptoethanol, 1x non-essential amino acids, 1 mM Na-pyruvate. MEFs were prepared from wild type and macroH2A1 null mice (Boulard et al., 2010) using standard methods. Briefly, 13,5-14,5 days old embryos were collected, cleaned with PBS, and processed (removal of the head, red tissues). The remaining embryos were minced and incubated in trypsin solution for 5 min at 37°c. Cells that remain in suspension were transferred in pre-warmed medium, washed one times in the same buffer and then plated in a 150 mm plate. Gene transduction with retroviral vectors was performed as described (Cantariño et al., 2016). Transduced cells were selected with 2μg/ml puromycin and 150 μg/ml hygromycin. Mouse E14 embryonic stem cells carrying stable shRNA cassettes were described before (Creppe et al., 2012a).

Antibodies and plasmids

We made use of the following antibodies: anti-IgG (Abcam, ab46540; ChIP: 3μg for 30 μg of chromatin), anti-H3 C-terminal (Abcam, ab1791; ChIP: 1μg for 30 μg of chromatin), anti-H3K9me3 (Abcam, ab8898; ChIP: 3μg for 30 μg of chromatin; IF: 1/100), anti-H3K9me3, mouse monoclonal (Sigma, SAB4800018, PLA:1/200), anti-nucleophosmin (Abcam, ab10530; IF: 1/100), anti-H3K27me3 (Millipore, 07-449, batch 2194165; ChIP: 3μg for 30 μg of chromatin), ANTI-FLAG® M2 Affinity beads (Sigma-Aldrich, A2220; IP: 20μL for 1mL of nuclear extract lysate), anti-Lamin B1 rabbit polyclonal antibody (Santa Cruz Biotechnology, sc-20682 - clone H90; ChIP: 1μg for 30 μg of chromatin; IF: 1/100; PLA: 1/50), anti-lamin B1, mouse monoclonal, ThermoFischer (MA1-06103 - clone 119D5-F1; PLA: 1/50), anti-macroH2A1 and anti-macroH2A2 (Buschbeck et al., 2009). The specificity of macroH2A antibodies was verified in Western blot, chromatin immunoprecipitation and immunofluorescence (Supplemental Figure S1). We used previously described pRetroSUPER constructs for shRNA-mediated knockdown of macroH2A1 and macroH2A2 (Buschbeck et al., 2009). The shRNA cassette directed against macroH2A2 was shuttled into a pRetroSUPER-hygromycin resistant backbone to permit the generation of macroH2A1/2 double knockdown. Two different Lamin B1-specific shRNAs expressed from lentiviral PLKO.1-puro backbone were ordered from SIGMA: shRNA#1:CCGGGCTCAAAGAAGTACAGTCTTTCTCGAGAAAGACTGTACTTC TTTGAGCTTTTTG, shRNA#2:CCGGCGCTTGAAGAACACTTCTGAACTCGAGTTCAGAAGTGTT CTTCAAGCGTTTTT.

Transmission electron microscopy

Cells were washed in PBS (pH 7.2) and fixed in 1.6 % glutaraldehyde diluted in 0.1M PBS (pH 7.2) at room temperature; after 1 h, they were washed in the same buffer. The samples were acetylated according to Thiry et al. (Thiry et al., 1985) before being embedded in Epon. Ultrathin sections mounted on copper grids were stained with uranyl acetate and lead citrate before examination with a Jeol JEM 1400 transmission electron microscope (TEM) at 80 kV.

Immunofluorescence staining, FISH and PLA

For immunofluorescence stainings, cells were grown in polylysine slides and fixed in PBS 4% PFA for 10min at RT, permeabilized in HCl 0.1M 0.5% Triton X-100 for 10min at RT and blocked with PBS 0.1% Tween (PBT) 5% BSA for 1h at RT. Primary antibodies were diluted in PBT 5% BSA and incubated for 1h at RT. After successive washes with PBT, secondary antibodies conjugated to Alexa 488 or 594 (Thermo Fischer) were diluted in PBT 5% BSA and incubated for 30min. After successive washes with PBT and PBS, slides were mounted with Vectashield® Mounting Medium with DAPI. Fluorescence *in situ* hybridizations (FISH) and slide preparations and was performed as described (Bolland et al., 2013). FISH probes were PCR-labeled using dUTP-biotin (Roche) and detected with streptavidin conjugated to Alexa 488 (Thermo Fischer) or Tyramide Signal Amplification (Thermo Fischer). For proximity ligation assay (PLA), cells were grown on 12mm coverslips. Prior to fixation in PBS 4% PFA for 10min at RT, cytoplasm was removed with CSK buffer (100 mM NaCl, 300 mM sucrose, 3 mM MgCl2, 10 mM PIPES + leupeptin 1:200 +PMSF 1:100) 5min on ice. Nuclei were permeabilized in HCl 0.1M 0.5% Triton X-100 for 10min at RT and blocked with PBS 0.1% Tween (PBT) 5% BSA for 30h at RT. Primary antibodies were diluted in PBT 5% BSA at a concentration of 10ng/µl and incubated for overnight at 4°C. Then, detection of protein interactions was performed using the Duolink system (Sigma-Aldrich) according to the manufacturer's instructions.

Microscopy, image acquisition and analysis

Confocal optical Z-stacks of images were obtained using a Zeiss LSM 710 confocal laser-scanning microscope equipped with a 63x/1.4 Plan-Apochromat oil immersion objective. Fluorochromes were excited with the following laser lines: 405nm (for DAPI detection), 488nm (for Alexa 488 detection) and 594nm (for Alexa 594 detection). Laser intensity and gain parameters were set to ensure proper exposure without saturated pixels. Ribosomal DNA FISH images were obtained using a Zeiss AxioObserver Z1 fluorescence microscope equipped with a 63x/1.4 Plan-Apochromat oil immersion objective. All acquisition parameters were kept equal during imaging of each experiment. Images were loaded and analysed in Fiji, a distribution of ImageJ (Schindelin et al., 2012), using custom macro scripts. Briefly, image stacks were converted to maximum intensity Z-projections, background was subtracted with a rolling ball algorithm and the signal was

automatically thresholded with built-in methods. Artifacts were removed after thresholding with noise removal and binary processing functions of the software. Nuclei, FISH spots and H3K9me3 foci were automatically identified with particle analyser and measured. Nucleoli were manually segmented from maximum intensity Z-projections of NPM1 immunostaining images. For the PLA experiment, 3D stack-images were acquired by confocal microscopy. Then, cell nuclei were segmented from the DAPI channel Z-stacks using automatic threshold (default built-in method) and a watershed algorithm. PLA signal blobs were identified from the green channel image stacks and assigned to the corresponding segmented nuclei with the FindFoci plugin (Herbert et al., 2014) with optimized parameters. All images of the different experimental conditions were analyzed under the same parameters.

ChIP, RT-qPCR and FAIRE

Chromatin immunoprecipitation (ChIP) experiments were performed and analysed essentially as previously described (Buschbeck et al., 2009). ChIP results are given as the percentage of ChIP over 10% of input material. Formaldehyde-assisted isolation of regulatory elements (FAIRE) assay was performed as described in (Simon et al., 2012). Regions of interest were analyzed by qPCR. All primers are listed in Supplemental Material Table S2.

ChIP-seq and association analysis

ChIP-seq data has been deposited in GEO under accession number GSE58175. DNA enriched by ChIP was fluorometrically quantified with PicoGreen and 10 ng were used for library preparation. Library generation and direct massive parallel sequencing on an Illumina genome analyser were performed according to the supplier's instructions at the core facility of EMBL (Heidelberg, Germany). The reads obtained were cleaned based on quality and trimmed using Sickle (Joshi and Fass) and Cutadapt (Martin, 2011), aligned versus human genome (GRCh37/hg19) using Bowtie 2 (Langmead and Salzberg, 2012) version 2.0.6, with *sensitive* preset option (*-D 15 -R 2 -L 22 -i S,1,1.15*). To detect genomic regions enriched for multiple overlapping (peaks) MACS software version 1.4.2 was used (Zhang et al., 2008) a p-value cutoff of 1.0e-5 and a FDR of 5% were used. The enrichment profiles were calculated using ngsplot ver 2.0 program (Shen et al., 2014). Screenshots of regions of interest were taken from the UCSC genome browser (Karolchik et al., 2013). A list of all shown positions is given in supplementary Table S1. To calculate the association between regions (peaks or DNA elements) we used regioneR, an R package based on permutation tests (Gel et al., 2015). To compare the associations between them, the z-score calculated were normalized by dividing them by $\sqrt{n}$ in which n refers to the number of regions in the region sets tested. We have further analyzed the following data sets generated by the ENCODE Project Consortium (Consortium, 2012): HepG 2x75 Sg 2 RNA-seq (GEO: GSM958732; UCSC: wgEncodeEH000127); HepG2 H3K9m3 (GEO: GSM1003519; UCSC: wgEncodeEH003087);

HepG2 H3K27m3 (GEO: GSM733754; UCSC: wgEncodeEH001023); and Repeatmasker (Smit et al.).

To calculate the coverage of ChIP-seq reads around LAD borders, we used deepTools software v2.2.2 (Ramirez et al., 2014). The coverage is expressed as the $\log_2$ ratio between signal and input normalized by the RPKM for a region centered on LAD borders +/- 100kb with a 2 kb sized bin. We have used LAD borders previously defined with a LMNB1 ChIP-seq in human IMR90 cells (Shah et al., 2013).

Analysis of proteins and post-translational modifications

Standard lysis and Western blot analyses were performed as previously described (Buschbeck et al., 2009). For immunoprecipitation (IP) of FLAG-tagged macroH2A1.2, 2 P10 plates cells stably expressing FLAG-MacroH2A1.2 were collected lysed with 0.32 M sucrose containing 0.1% Triton buffer and intact nuclei were resuspended in 500µL EX100 buffer+2mM CaCL2. Extracts were digested with 5U of MNase 20 min at 26°C, reaction stopped with 1/50 EGTA 0,5M. Supernatants were collected after centrifugation 5min 1000g. Remaining pellets were resuspended in EX100 buffer, sonicated with Bioruptor (2 min, high intensity, 30sec on-30sec off) and pooled with supernatants. After the pre-clearing with slurry sepharose beads (Sigma), input sample was collected and 20 µL FLAG-bead slurry (Sigma) were added to each replicate. After 2h incubation, Flag-beads were washed and the technical replicates were joint and resuspended in 50µL laemmli buffer. pH was adjusted with 0.5M Tris pH6.8. For western blot, 0.5% input 20% IP material were loaded. Pure modified histone H3 proteins generated by chemical ligation were kindly provided by Till Bartke (Imperial College London, UK) and used as reference samples (Bartke et al., 2010).

Statistics

Unless indicated otherwise, RT-qPCR and ChIP data is represented as the mean of at least three independent experiments, errors bars denote the standard error of the mean (SEM). Statistical tests used to calculate p-values are given stated in the figure legends.

ACKNOWLEDGEMENTS

We thank Till Bartke for essential tools, P. Piscicelli for the preparation of TEM samples and Hélène Delage for technical support.

FUNDING

This work was supported by grants from MINECO (BFU2015-66559-P), the Deutsche José Carreras Leukaemie Stiftung (DJCLS R 14/16), AFM Téléthon (AFM 18738), the Marie Skłodowska Curie Training network 'ChroMe' (H2020-MSCA-ITN-2015-675610), AGAUR (2014-SGR-35). DC was supported by a MECD-funded FPU fellowship (FPU14/06542). VS was funded by a Marie Curie Fellowship (INTEGER 214902) and a grant from the European Network of Excellence grant (EpiGeneSys 257082). NC was supported by a FPI PhD fellowship (BES-2010-031876), and JD by a Juan de la Cierva fellowship (JCI-2011-10831). Research leading to inventions at the IJC is supported by the 'La Caixa' Foundation, the Fundació Internacional Josep Carreras, Celgene Spain and the CERCA Programme / Generalitat de Catalunya.

ABBREVIATIONS

ChIP, chromatin IP

FISH, Fluorescence in situ Hybridization

LAD, lamin-associated domain

LMNB1, Lamin B1

mH2A, macroH2A

NPM1, nucleophosmin 1

PLA, proximity ligation assay

s.e.m., standard error of the mean

REFERENCES

Amendola, M. and van Steensel, B. (2014). Mechanisms and dynamics of nuclear lamina. *Current Opinion in Cell Biology* **28**, 61–68.

Barrero, M. J., Sese, B., Marti, M. and Izpisua Belmonte, J. C. (2013a). Macro Histone Variants Are Critical for the Differentiation of Human Pluripotent Cells. *Journal of Biological Chemistry* **288**, 16110–16116.

Barrero, M. J., Sesé, B., Kuebler, B., Bilic, J., Boue, S., Martí, M. and Belmonte, J. C. I. (2013b). Macrohistone Variants Preserve Cell Identity by Preventing the Gain of H3K4me2 during Reprogramming to Pluripotency. *CellReports* **3**, 1005–1011.

Bartke, T., Vermeulen, M., Xhemalce, B., Robson, S. C., Mann, M. and Kouzarides, T. (2010). Nucleosome-Interacting Proteins Regulated by DNA and Histone Methylation. *Cell* **143**, 470–484.

Bian, Q., Khanna, N., Alvikas, J. and Belmont, A. S. (2013). β-Globin cis-elements determine differential nuclear targeting through epigenetic modifications. *The Journal of Cell Biology* **203**, 767–783.

Bolland, D. J., King, M. R., Reik, W., Corcoran, A. E. and Krueger, C. (2013). Robust 3D DNA FISH Using Directly Labeled Probes. *JoVE*.

Boulard, M., Storck, S., Cong, R., Pinto, R., Delage, H. and Bouvet, P. (2010). Histone variant macroH2A1 deletion in mice causes female-specific steatosis. *Epigenetics & Chromatin* **3**, 8.

Bouzinba-Segard, H., Guais, A. and Francastel, C. (2006). Accumulation of small murine minor satellite transcripts leads to impaired centromeric architecture and function. *Proc. Natl. Acad. Sci. U.S.A.* **103**, 8709–8714.

Buschbeck, M., Uribesalgo, I., Wibowo, I., Rué, P., Martin, D., Gutiérrez, A., Morey, L., Guigó, R., López-Schier, H. and Di Croce, L. (2009). The histone variant macroH2A is an epigenetic regulator of key developmental genes. *Nature Structural & Molecular Biology* **16**, 1074–1079.

Cantariño, N., Douet, J. and Buschbeck, M. (2013). MacroH2A – An epigenetic regulator of cancer. *Cancer Letters* **336**, 247–252.

Cantariño, N., Fernández-Figueras, M. T., Valero, V., Musulen, E., Malinverni, R., Granada, I., Goldie, S. J., Martín-Caballero, J., Douet, J., Forcales, S. V., et al. (2016). A cellular model reflecting the phenotypic heterogeneity of mutant HRASdriven squamous cell carcinoma. *Int. J. Cancer*.

Cesarini, E., Mozzetta, C., Marullo, F., Gregoretti, F., Gargiulo, A., Columbaro, M., Cortesi, A., Antonelli, L., Di Pelino, S., Squarzoni, S., et al. (2015). Lamin A/C sustains PcG protein architecture, maintaining transcriptional repression at target genes. *The Journal of Cell Biology* **211**, 533–551.

Chadwick, B. P. (2008). DXZ4 chromatin adopts an opposing conformation to that of the surrounding chromosome and acquires a novel inactive X-specific role involving CTCF and antisense transcripts. *Genome Research* **18**, 1259–1269.

Chadwick, B. P. and Willard, H. F. (2004). Multiple spatially distinct types of facultative heterochromatin on the human inactive X chromosome. *Proc. Natl. Acad. Sci. U.S.A.* **101**, 17450–17455.

Changolkar, L. N. and Pehrson, J. R. (2006). macroH2A1 Histone Variants Are Depleted on Active Genes but Concentrated on the Inactive X Chromosome. *Molecular and Cellular Biology* **26**, 4410–4420.

Changolkar, L. N., Singh, G., Cui, K., Berletch, J. B., Zhao, K., Disteche, C. M. and Pehrson, J. R. (2010). Genome-Wide Distribution of MacroH2A1 Histone Variants in Mouse Liver Chromatin. *Molecular and Cellular Biology* **30**, 5473–5483.

Chen, H., Ruiz, P. D., Novikov, L., Casill, A. D., Park, J. W. and Gamble, M. J. (2014). MacroH2A1.1 and PARP-1 cooperate to regulate transcription by promoting CBP-mediated H2B acetylation. *Nature Structural & Molecular Biology* **21**, 981–989.

Cong, R., Das, S., Douet, J., Wong, J., Buschbeck, M., Mongelard, F. and Bouvet, P. (2013). macroH2A1 histone variant represses rDNA transcription. *Nucleic Acids Research* **42**, 181–192.

Consortium, T. E. P. (2012). An integrated encyclopedia of DNA elements in the human genome. *Nature* **488**, 57–74.

Creppe, C., Janich, P., Cantarino, N., Noguera, M., Valero, V., Musulen, E., Douet, J., Posavec, M., Martin-Caballero, J., Sumoy, L., et al. (2012a). MacroH2A1 Regulates the Balance between Self-Renewal and Differentiation Commitment in Embryonic and Adult Stem Cells. *Molecular and Cellular Biology* **32**, 1442–1452.

Creppe, C., Posavec, M., Douet, J. and Buschbeck, M. (2012b). MacroH2A in stem cells: a story beyond gene repression. *Epigenomics* **4**, 221–227.

Diesch, J., Hannan, R. D. and Sanij, E. (2014). Perturbations at the ribosomal genes loci are at the centre of cellular dysfunction and human disease. *Cell Biosci* **4**, 43.

Diez, A., Bernat, G., Buschbeck, M., Serra, E., Peinado, M. A. and Malinverni, R. (2014). *regioneR: an R/Bioconductor package for the magement and comparision of genomic regions.* Bioinformatics.

Freund, A., Laberge, R. M., Demaria, M. and Campisi, J. (2012). Lamin B1 loss is a senescence-associated biomarker. *Mol. Biol. Cell* **23**, 2066–2075.

Fu, Y., Lv, P., Yan, G., Fan, H., Cheng, L., Zhang, F., Dang, Y., Wu, H. and Wen, B. (2015). MacroH2A1 associates with nuclear lamina and maintains chromatin architecture in mouse liver cells. *Sci. Rep.* 1–12.

Gamble, M. J., Frizzell, K. M., Yang, C., Krishnakumar, R. and Kraus, W. L. (2010). The histone variant macroH2A1 marks repressed autosomal chromatin, but protects a subset of its target genes from silencing. *Genes & Development* **24**, 21–32.

Gaspar-Maia, A., Qadeer, Z. A., Hasson, D., Ratnakumar, K., Leu, N. A., LeRoy, G., Liu, S., Costanzi, C., Valle-Garcia, D., Schaniel, C., et al. (2013). MacroH2A histone variants act as a barrier upon reprogramming towards pluripotency. *Nature Communications* **4**, 1565–12.

Gel, B., Diez-Villanueva, A., Serra, E., Buschbeck, M., Peinado, M. A. and Malinverni, R. (2015). regioneR: an R/Bioconductor package for the association analysis of genomic regions based on permutation tests. *Bioinformatics* btv562.

Gesson, K., Rescheneder, P., Skoruppa, M. P., Haeseler, von, A., Dechat, T. and Foisner, R. (2016). A-type lamins bind both hetero- and euchromatin, the latter being regulated by lamina-associated polypeptide 2 alpha. *Genome Research* **26**, 462–473.

Gonzalez-Sandoval, A., Towbin, B. D., Kalck, V., Cabianca, D. S., Gaidatzis, D., Hauer, M. H., Geng, L., Wang, L., Yang, T., Wang, X., et al. (2015). Perinuclear Anchoring of H3K9-Methylated Chromatin Stabilizes Induced Cell Fate in C. elegans Embryos. *Cell* 1–16.

Gruenbaum, Y. and Medalia, O. (2015). ScienceDirectLamins: the structure and protein complexes. *Current Opinion in Cell Biology* **32**, 7–12.

Guelen, L., Pagie, L., Brasset, E., Meuleman, W., Faza, M. B., Talhout, W., Eussen, B. H., de Klein, A., Wessels, L., de Laat, W., et al. (2008). Domain organization of human chromosomes revealed by mapping of nuclear lamina interactions. *Nature* **453**, 948–951.

Harr, J. C., Luperchio, T. R., Wong, X., Cohen, E., Wheelan, S. J. and Reddy, K. L. (2015). Directed targeting of chromatin to the nuclear lamina is mediated by chromatin state and A-type lamins. *The Journal of Cell Biology* **208**, 33–52.

Herbert, A. D., Carr, A. M. and Hoffmann, E. (2014). FindFoci: A Focus Detection Algorithm with Automated Parameter Training That Closely Matches Human Assignments, Reduces Human Inconsistencies and Increases Speed of Analysis. *PLoS ONE* **9**, e114749.

Hernández-Muñoz, I., Lund, A. H., van der Stoop, P., Boutsma, E., Muijrers, I., Verhoeven, E., Nusinow, D. A., Panning, B., Marahrens, Y. and van Lohuizen, M. (2005). Stable X chromosome inactivation involves the PRC1 Polycomb complex and requires histone MACROH2A1 and the CULLIN3/SPOP ubiquitin E3 ligase. *Proc. Natl. Acad. Sci. U.S.A.* **102**, 7635–7640.

Joshi, N. A. and Fass, J. A. Sickle: A sliding-window, adaptive, quality-based trimming tool for FastQ files (Version 1.21).

Kapoor, A., Goldberg, M. S., Cumberland, L. K., Ratnakumar, K., Segura, M. F., Emanuel, P. O., Menendez, S., Vardabasso, C., LeRoy, G., Vidal, C. I., et al. (2010). The histone variant macroH2A suppresses melanoma progression through regulation of CDK8. *Nature* **468**, 1105–1109.

Karolchik, D., Barber, G. P., Casper, J., Clawson, H., Cline, M. S., Diekhans, M., Dreszer, T. R., Fujita, P. A., Guruvadoo, L., Haeussler, M., et al. (2013). The UCSC Genome Browser database: 2014 update. *Nucleic Acids Research* **42**, D764–D770.

Kind, J., Pagie, L., de Vries, S. S., Nahidiazar, L., Dey, S. S., Bienko, M., Zhan, Y., Lajoie, B., de Graaf, C. A., Amendola, M., et al. (2015). Genome-wide Maps of Nuclear Lamina Interactions in Single Human Cells. *Cell* 1–15.

Kind, J., Pagie, L., Ortabozkoyun, H., Boyle, S., de Vries, S. S., Janssen, H., Amendola, M., Nolen, L. D., Bickmore, W. A. and van Steensel, B. (2013). Single-Cell Dynamics of Genome-Nuclear Lamina Interactions. *Cell* **153**, 178–192.

Langmead, B. and Salzberg, S. L. (2012). Fast gapped-read alignment with Bowtie 2. *Nature Methods* **9**, 357–359.

Lavigne, M. D., Vatsellas, G., Polyzos, A., Mantouvalou, E., Sianidis, G., Maraziotis, I., Agelopoulos, M. and Thanos, D. (2015). Composite macroH2A/NRF-1 Nucleosomes Suppress Noise and Generate Robustness in Gene Expression. *CellReports* **11**, 1090–1101.

Maison, C. and Almouzni, G. (2004). HP1 and the dynamics of heterochromatin maintenance. *Nature Reviews Molecular Cell Biology* **5**, 296–305.

Martin, C., Chen, S., Maya-Mendoza, A., Lovric, J., Sims, P. F. G. and Jackson, D. A. (2009). Lamin B1 maintains the functional plasticity of nucleoli. *Journal of Cell Science* **122**, 1551–1562.

Martin, M. (2011). Cutadapt removes adapter sequences from high-throughput sequencing reads. *EMBnet. journal* **17**, pp. 10–12.

Meuleman, W., Peric-Hupkes, D., Kind, J., Beaudry, J. B., Pagie, L., Kellis, M., Reinders, M., Wessels, L. and van Steensel, B. (2013). Constitutive nuclear lamina-genome interactions are highly conserved and associated with A/T-rich sequence. *Genome Research* **23**, 270–280.

Muthurajan, U. M., McBryant, S. J., Lu, X., Hansen, J. C. and Luger, K. (2011). The Linker Region of MacroH2A Promotes Self-association of Nucleosomal Arrays. *Journal of Biological Chemistry* **286**, 23852–23864.

Németh, A., Conesa, A., Santoyo-Lopez, J., Medina, I., Montaner, D., Péterfia, B., Solovei, I., Cremer, T., Dopazo, J. and Längst, G. (2010). Initial Genomics of the Human Nucleolus. *PLoS Genet* **6**, e1000889.

Padeken, J., Zeller, P. and Gasser, S. M. (2015). ScienceDirectRepeat DNA in genome organization and stability. *Current Opinion in Genetics & Development* **31**, 12–19.

Park, S.-J., Shim, J. W., Park, H. S., Eum, D.-Y., Park, M.-T., Yi, J. M., Choi, S. H., Kim, S. D., Son, T. G., Lu, W., et al. (2015). MacroH2A1 downregulation enhances the stem-like propertiesof bladder cancer cells by transactivation of Lin28B. *Oncogene* **35**, 1292–1301.

Pasque, V., Gillich, A., Garrett, N. and Gurdon, J. B. (2011). Histone variant macroH2A confers resistance to nuclear reprogramming. *The EMBO Journal* **30**, 2373–2387.

Pasque, V., Radzisheuskaya, A., Gillich, A., Halley-Stott, R. P., Panamarova, M., Zernicka-Goetz, M., Surani, M. A. and Silva, J. C. R. (2013). Histone variant macroH2A marks embryonic differentiation in vivo and acts as an epigenetic barrier to induced pluripotency. *Journal of Cell Science* **125**, 6094–6104.

Pehrson, J. R., Changolkar, L. N., Costanzi, C. and Leu, N. A. (2014). Mice without MacroH2A Histone Variants. *Molecular and Cellular Biology* **34**, 4523–4533.

Pehrson, J. R., Costanzi, C. and Dharia, C. (1997). Developmental and tissue expression patterns of histone macroH2A1 subtypes. *J. Cell. Biochem.* **65**, 107–113.

Peters, A. H. F. M., Kubicek, S., Mechtler, K., O'Sullivan, R. J., Derijck, A. A. H. A., Perez-Burgos, L., Kohlmaier, A., Opravil, S., Tachibana, M., Shinkai, Y., et al. (2003). Partitioning and plasticity of repressive histone methylation states in mammalian chromatin. *Molecular Cell* **12**, 1577–1589.

Posavec, M., Timinszky, G. and Buschbeck, M. (2013). Macro domains as metabolite sensors on chromatin. *Cell. Mol. Life Sci.* **70**, 1509–1524.

Ramirez, F., Dundar, F., Diehl, S., Gruning, B. A. and Manke, T. (2014). deepTools: a flexible platform for exploring deep-sequencing data. *Nucleic Acids Research* **42**, W187–W191.

Rice, J. C., Briggs, S. D., Ueberheide, B., Barber, C. M., Shabanowitz, J., Hunt, D. F., Shinkai, Y. and Allis, C. D. (2003). Histone methyltransferases direct different degrees of methylation to define distinct chromatin domains. *Molecular Cell* **12**, 1591–1598.

Robson, M. I., las Heras, de, J. I., Czapiewski, R., Thành, P. L., Booth, D. G., Kelly, D. A., Webb, S., Kerr, A. R. W. and Schirmer, E. C. (2016). Tissue-Specific Gene Repositioning by Muscle Nuclear Membrane Proteins Enhances Repression of Critical Developmental Genes during Myogenesis. *Molecular Cell* **62**, 834–847.

Schindelin, J., Arganda-Carreras, I., Frise, E., Kaynig, V., Longair, M., Pietzsch, T., Preibisch, S., Rueden, C., Saalfeld, S., Schmid, B., et al. (2012). Fiji: an open-source platform for biological-image analysis. *Nature Methods* **9**, 676–682.

Shah, P. P., Donahue, G., Otte, G. L., Capell, B. C., Nelson, D. M., Cao, K., Aggarwala, V., Cruickshanks, H. A., Rai, T. S., McBryan, T., et al. (2013). Lamin B1 depletion in senescent cells triggers large-scale changes in gene expression and the chromatin landscape. *Genes & Development* **27**, 1787–1799.

Shen, L., Shao, N., Liu, X. and Nestler, E. (2014). ngs.plot: Quick mining and visualization of next-generation sequencing data by integrating genomic databases. *BMC Genomics* **15**, 1–14.

Simon, J. M., Giresi, P. G., Davis, I. J. and Lieb, J. D. (2012). Using formaldehyde-assisted isolation of regulatory elements (FAIRE) to isolate active regulatory DNA. *Nature Protocols* **7**, 256–267.

Smit, A., Hubley, R. and Green, P. RepeatMasker Open-4.0. 2013-2015.

Soufi, A., Donahue, G. and Zaret, K. S. (2012). Facilitators and Impediments of the Pluripotency Reprogramming Factors' Initial Engagement with the Genome. *Cell* **151**, 994–1004.

Sridharan, R., Gonzales-Cope, M., Chronis, C., Bonora, G., McKee, R., Huang, C., Patel, S., Lopez, D., Mishra, N., Pellegrini, M., et al. (2013). Proteomic and genomic approaches reveal critical functions of H3K9 methylation and heterochromatin protein-1 in reprogramming to pluripotency. *Nature Cell Biology* **15**, 872–882.

Taddei, A., Maison, C., Roche, D. and Almouzni, G. (2001). Reversible disruption of pericentric heterochromatin and centromere function by inhibiting deacetylases. *Nature Cell Biology* **3**, 114–120.

Thiry, M., Lepoint, A. and Goessens, G. (1985). Re-evaluation of the site of transcription in Ehrlich tumour cell nucleoli. *Biol. Cell* **54**, 57–64.

Towbin, B. D., González-Aguilera, C., Sack, R., Gaidatzis, D., Kalck, V., Meister, P., Askjaer, P. and Gasser, S. M. (2012). Step-wise methylation of histone H3K9 positions heterochromatin at the nuclear periphery. *Cell* **150**, 934–947.

Trojer, P. and Reinberg, D. (2007). Facultative heterochromatin: is there a distinctive molecular signature? *Molecular Cell* **28**, 1–13.

van Koningsbruggen, S., Gierlinski, M., Schofield, P., Martin, D., Barton, G. J., Ariyurek, Y., Dunnen, den, J. T. and Lamond, A. I. (2010). High-resolution whole-genome sequencing reveals that specific chromatin domains from most human chromosomes associate with nucleoli. *Mol. Biol. Cell* **21**, 3735–3748.

Xu, D., Li, C.-F., Zhang, X., Gong, Z., Chan, C.-H., Lee, S.-W., Jin, G., Rezaeian, A.-H., Han, F., Wang, J., et al. (2015). Skp2-macroH2A1-CDK8 axis orchestrates G2/M transition and tumorigenesis. *Nature Communications* **6**, 6641.

Yelagandula, R., Stroud, H., Holec, S., Zhou, K., Feng, S., Zhong, X., Muthurajan, U. M., Nie, X., Kawashima, T., Groth, M., et al. (2014). The Histone Variant H2A.W Defines Heterochromatin and Promotes Chromatin Condensation in Arabidopsis. *Cell* **158**, 98–109.

Zhang, R., Poustovoitov, M. V., Ye, X., Santos, H. A., Chen, W., Daganzo, S. M., Erzberger, J. P., Serebriiskii, I. G., Canutescu, A. A., Dunbrack, R. L., et al. (2005). Formation of MacroH2A-Containing Senescence-Associated Heterochromatin Foci and Senescence Driven by ASF1a and HIRA. *Developmental Cell* **8**, 19–30.

Zhang, Y., Liu, T., Meyer, C. A., Eeckhoute, J., Johnson, D. S., Bernstein, B. E., Nussbaum, C., Myers, R. M., Brown, M., Li, W., et al. (2008). Model-based Analysis of ChIP-Seq (MACS). *Genome Biol* **9**, R137.

Figures

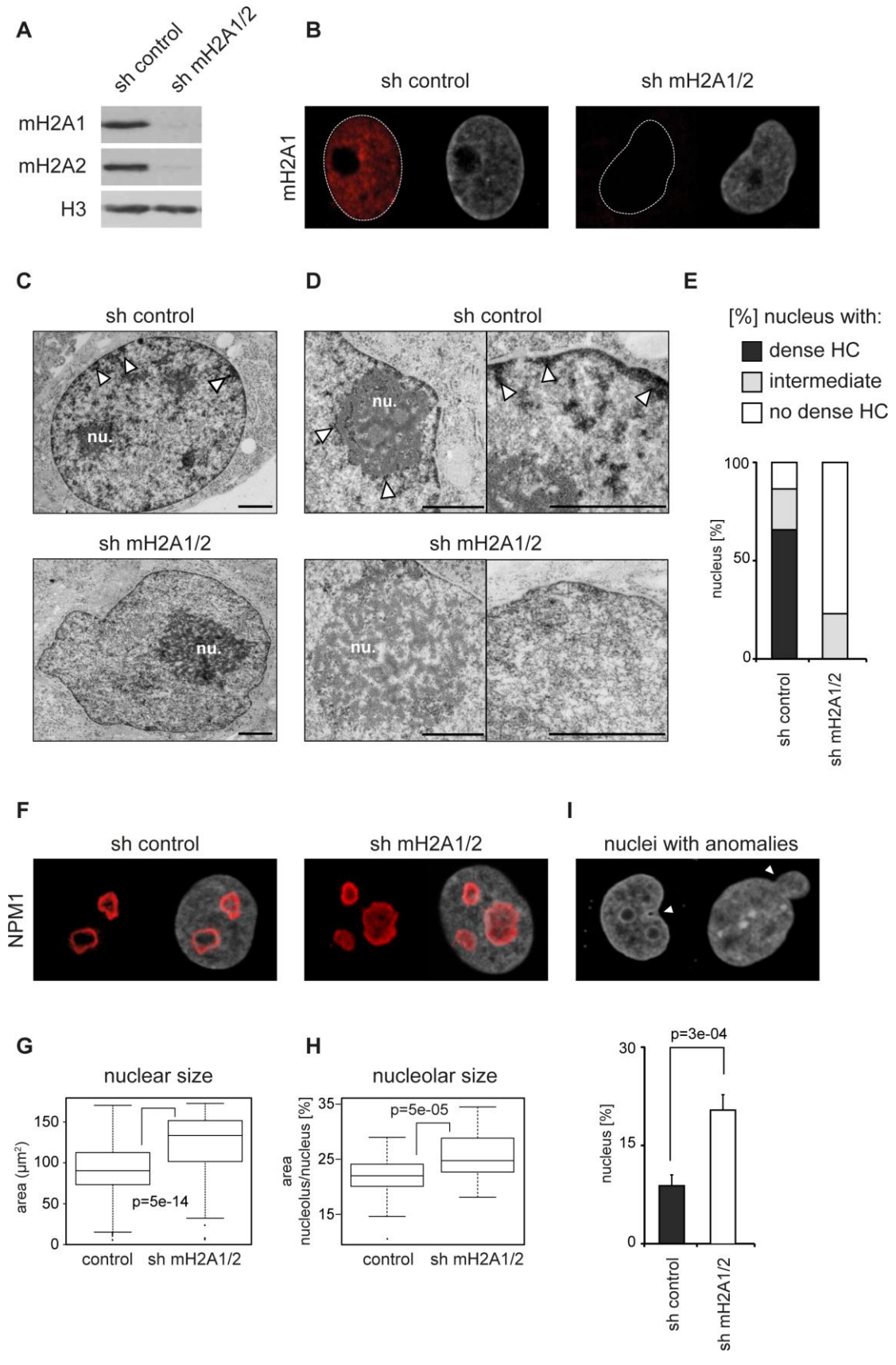

Figure 1. MacroH2A proteins are essential for proper nuclear and nucleolar organization.

(A) Western blot showing the stable depletion of macroH2A1 and macroH2A2 in HepG2 cells transduced with retroviral shRNA cassettes (sh mH2A1/2) in comparison to control cells (sh control). Immunoblotting of histone H3 has been included to ensure equivalent loading of protein.

(B) Immunostaining of macroH2A1 in control and knockdown HepG2 cells (red). Nuclei counterstained with DAPI (grey).

(C) Transmission electron microscopy analysis of HepG2 sh control cells (control) and sh macroH2A1/2 (sh mH2A1/2) knockdown cells. White arrowheads indicate dark contrast staining corresponding to dense heterochromatin and 'nu.' marks the nucleolus. Scale bar is 1 μM.

(D) Higher magnification of selected nuclei focusing on the nucleolus (nu.) the nuclear periphery. White arrow-heads indicate dense heterochromatin regions. Scale bar is 1 μM.

(E) Quantification of nuclei from C according to their heterochromatin content. Three classes were distinguished: dense, intermediate and no dense heterochromatin ($n > 100$).

(F) Immunostaining of nucleophosmin (NPM1) in control and knockdown HepG2 cells (red). Nuclei were counterstained with DAPI (grey).

(G) Quantification of the nuclear surface in control and knockdown HepG2 cells ($n > 100$) stained as in F. Wilcoxon rank sum test was used to compare the two groups.

(H) Percentage of nuclear area occupied by the nucleolus (identified by NPM1 detection) in nuclei from F. Wilcoxon rank sum test was used to compare control ($n=49$) and knockdown samples ($n=51$).

(I) The proportion of nuclei presenting anomalies such as bud-like structures and cavities (examples shown in the left panel) in control and knockdown HepG2 cells has been quantified ($n > 200$). P-value was calculated by two-tailed Z-test.

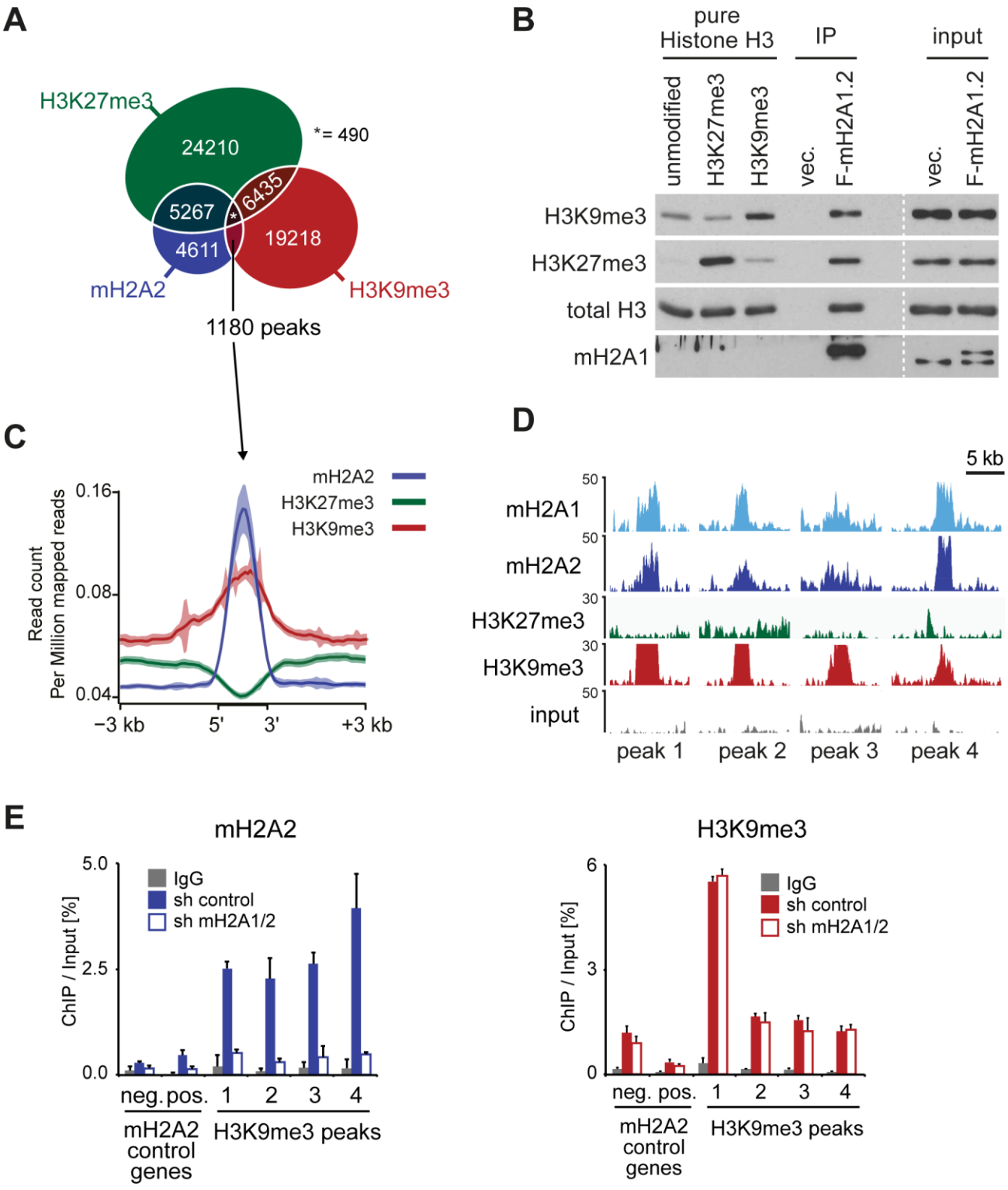

Figure 2. MacroH2A associates with the H3K9me3 mark.

(A) Venn diagram showing the overlap of macroH2A2 (mH2A2) peaks with H3K9me3 and H3K27me3 peaks in HepG2 cells. The number of peaks is indicated.

(B) Anti-FLAG-affinity precipitation of mH2A1.2-containing nucleosomes in HepG2 cells stably expressing FLAG (F)-mH2A1.2 or containing empty vector (vec.). The amount of H3K27me3 and H3K9me3 of co-precipitated histone H3 was analyzed by immunoblotting. Pure modified histone H3 proteins generated by chemical ligation (Bartke et al., 2010) were included as reference samples.

(C) Normalized read distribution of macroH2A2, H3K27me3 and H3K9me3 reads around 1180 mH2A2 peaks identified in A overlap with H3K9me3 but not H3K27me3. The region between the 5' and 3' borders of the peaks has been scaled and is plotted in the same size for all peaks.

(D) Four examples of macroH2A peak enrichments associated with H3K9me3 in HepG2 cells. Snapshots from the UCSC genome are shown for macroH2A1, macroH2A2, H3K27me3, H3K9me3 and input in HepG2 cells. Coordinates of the snapshots are provided in Table S1.

(E) Occupancy of macroH2A2 and H3K9me3 on the same interstitial heterochromatin peaks shown in D was analyzed by ChIP in control cells (sh control) and cells deficient of both macroH2A proteins (sh mH2A1/2). The upstream promoter regions of *LAMA5* and *GRXCR1* served as positive and negative controls, respectively, for macroH2A2-enrichment. Data is shown as mean of three experiments+SEM.

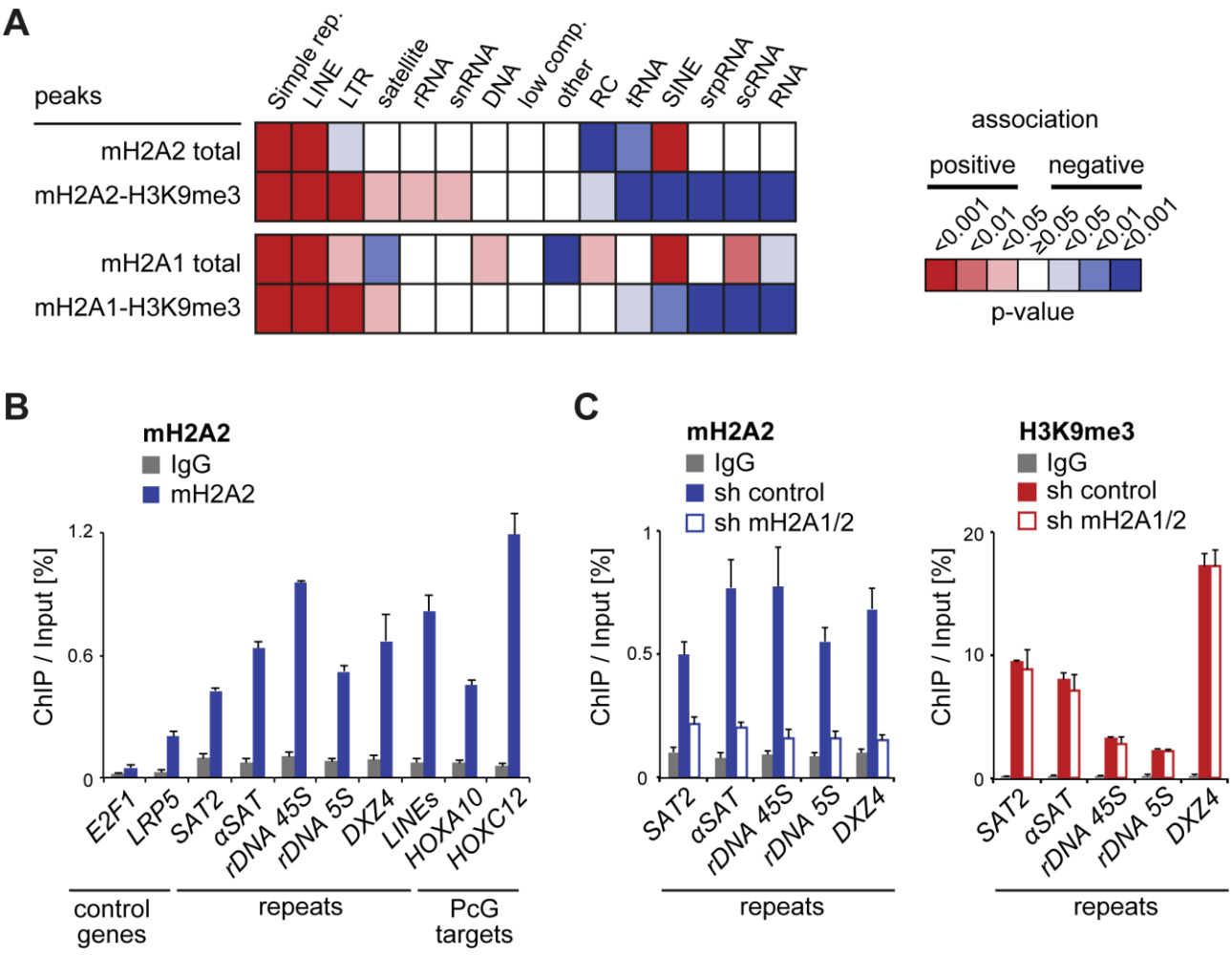

Figure 3. MacroH2A2 is enriched on constitutive heterochromatin repeats.

(A) The chart summarizes the association of macroH2A2 (mH2A2) and mH2A2-H3K9me3 enriched regions in HepG2 with repeat classes indexed in Repeatmasker. Association was calculated with the permutation-test based R-package regioneR (Diez et al., 2014) performing 1000 iterations. Color grading correlates with p-values and blue and red colors denote negative and positive association, respectively.

(B) The level of mH2A2 enrichments on various repeats and on a set of lowly enriched control genes (*E2F1*, *LRP5)* and highly enriched Polycomb (PcG) target genes (*HOXA10*, *HOXC12*) was analyzed by ChIP-qPCR. IgG was used as background control. Data is shown as mean + s.e.m. (n=3).

(C) mH2A2 and H3K9me3 occupancy on pericentromeric satellite repeats (*SAT2*, *αSAT*), ribosomal DNA (*45S* and *5S*), and *DXZ4* repeat analyzed by ChIP in control and macroH2A knockdown HepG2 cells (sh control and sh mH2A1/2, respectively). Results were normalized by histone H3 ChIP and IgG was used as background control. Data is shown as mean + s.e.m. (n=3).

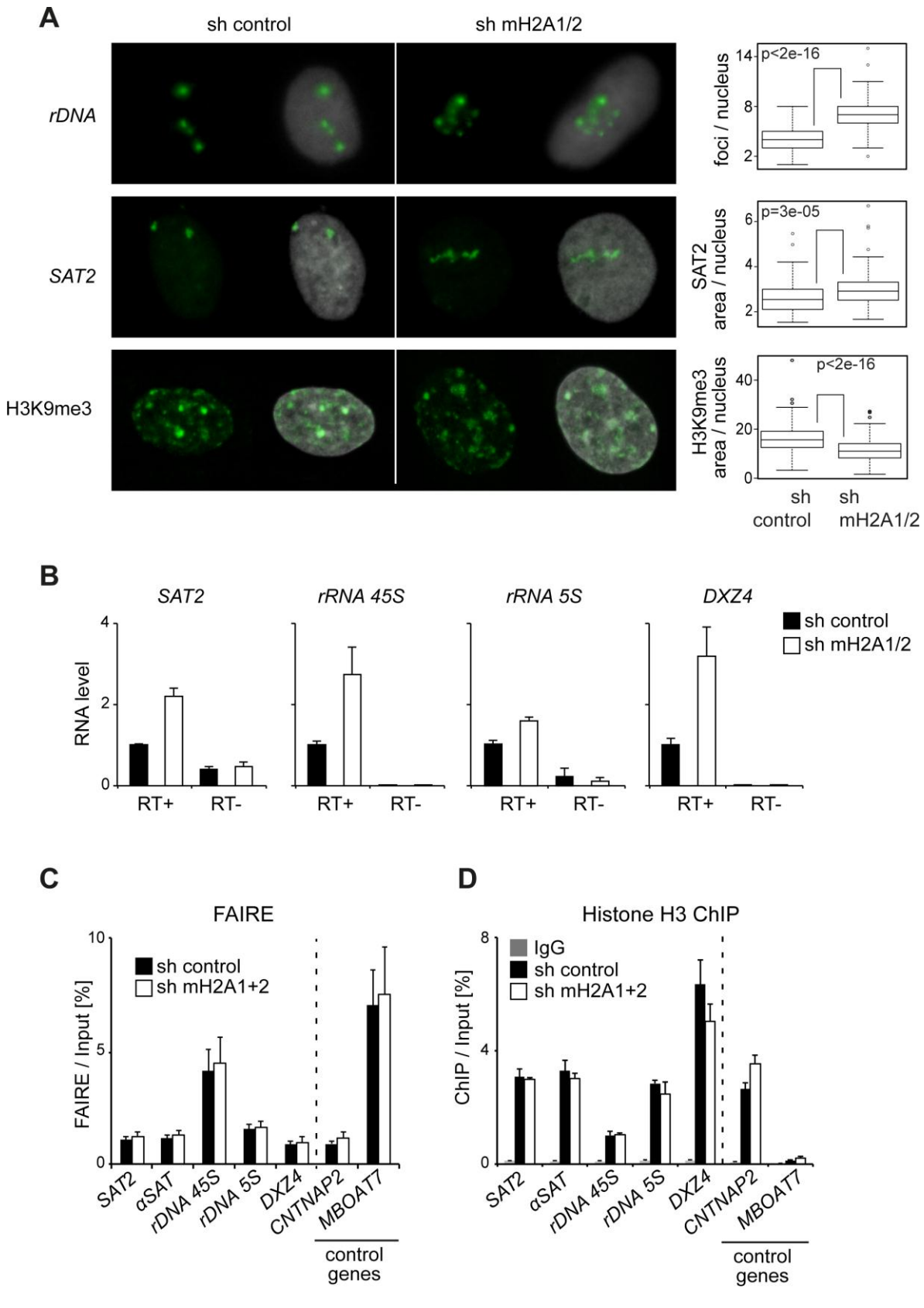

Figure 4. MacroH2A maintains heterochromatic architecture.

(A) Fluorescent *in situ* hybridization of *rDNA 45S* and *SAT2* (upper and middle panel) and H3K9me3 immunostainig (bottom panel) on nuclei from HepG2 control cells and sh mH2A1/2 are shown in green. Nuclei were counterstained with DAPI (grey). On the right quantifications are given in box plots. Top; number of rDNA foci detected per nucleus in control and knockdown conditions (control, n=81; sh mH2A1/2, n=62). Middle; fraction of the nucleus occupied by *SAT2* repeats in % of nucleus area (control n=79; sh mH2A1/2 n=125). Bottom; fraction of the nucleus occupied by H3K9me3 domains in % of nucleus area (control n=229; sh mH2A1/2 n=215).

(B) RT-qPCR analysis of RNA levels in the same cells. Levels in control cells have been set to one. Reactions without reverse transcriptase have been included to determine the background of the detection method (RT-). Values were normalized to the expression of the two housekeeping genes *RPO and GAPDH*. Data is shown as mean + s.e.m. (n=3).

(C) Local openness of repeats assayed by FAIRE in sh control and sh mH2A1/2 HepG2 cells. Data is plotted as percentage of FAIRE-extracted DNA in respect to DNA from input material. The genes *CNTNAP2* and *MBOAT7* have been included as previously described closed and open control loci, respectively (Simon et al., 2012). Data is shown as mean + s.e.m. (n=3).

(D) H3 occupancy on repeats assayed by ChIP in HepG2 control cells and sh mH2A1/2 knockdown cells. The same loci as in (C) were used as controls. Data is shown as mean + s.e.m. (n=3).

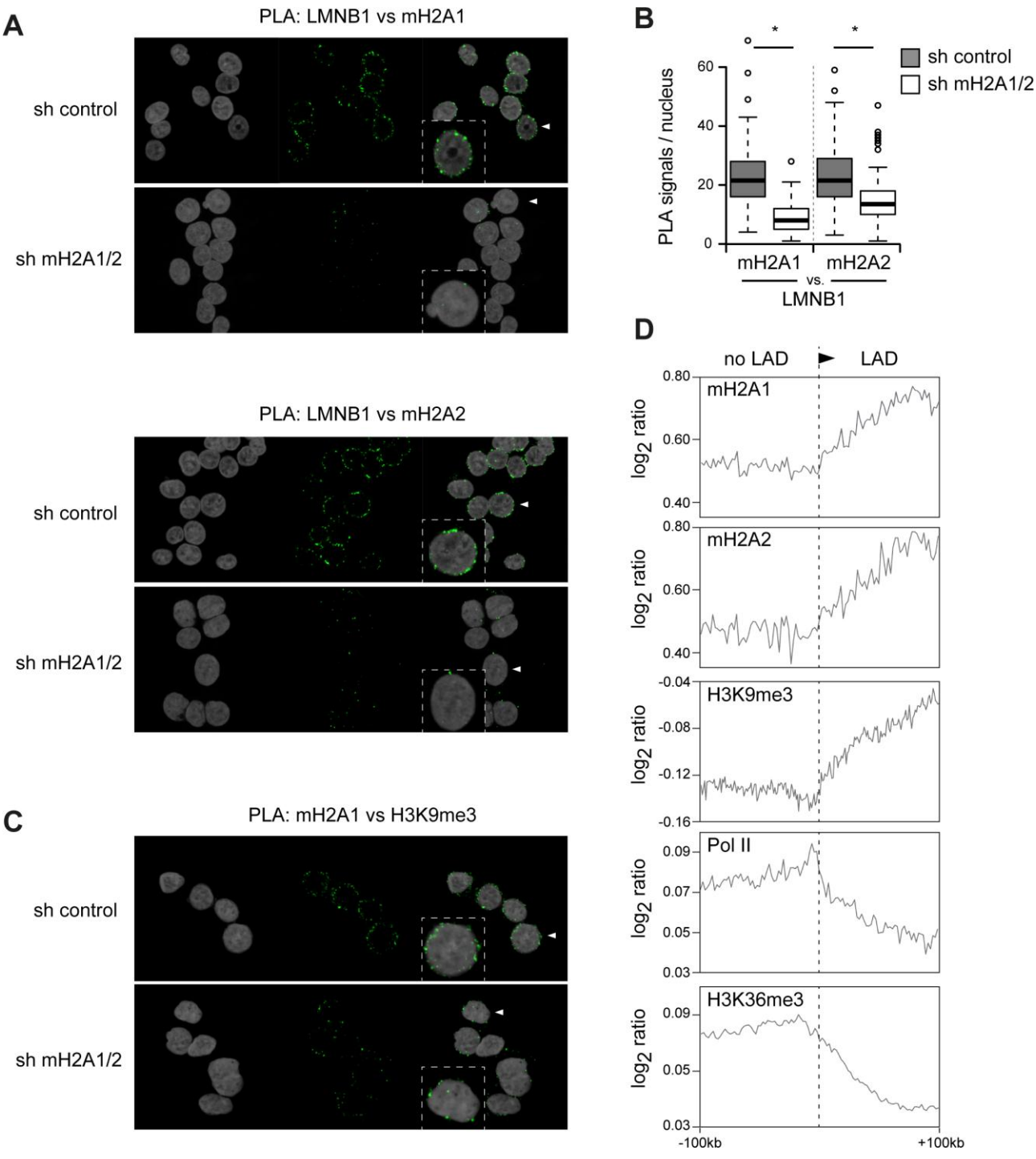

Figure 5. MacroH2A proteins interact with Lamin B1.

(A) Detection of Lamin B1 (LMNB1) – macroH2A interaction by proximity ligation assay (PLA) in control HepG2 cells and sh mH2A1/2 cells. PLAs with LMNB1 antibody alone and in combination with a different LMNB1 antibody were included as negative and positive controls, respectively (Supplemental Figure S6). Cells were counterstained with DAPI.

(B) Quantification of detected PLA signals per nucleus in the images obtained in A; n ≥ 100. Wilcoxon rank sum test was used to compare the control and sh mH2A1/2 groups, n ≥ 100.

(C) Detection of H3K9me3 – macroH2A1 interaction by PLA in control HepG2 cells and sh mH2A1/2 cells. Cells were counterstained with DAPI.

(D) Plots show normalized read coverage of different marks over 1962 previously defined LAD borders (Shah et al., 2013). Coverage is expressed as the $\log_2$ ratio between signal and input normalized by the RPKM. Dashed line marks the 5' border of the LADs.

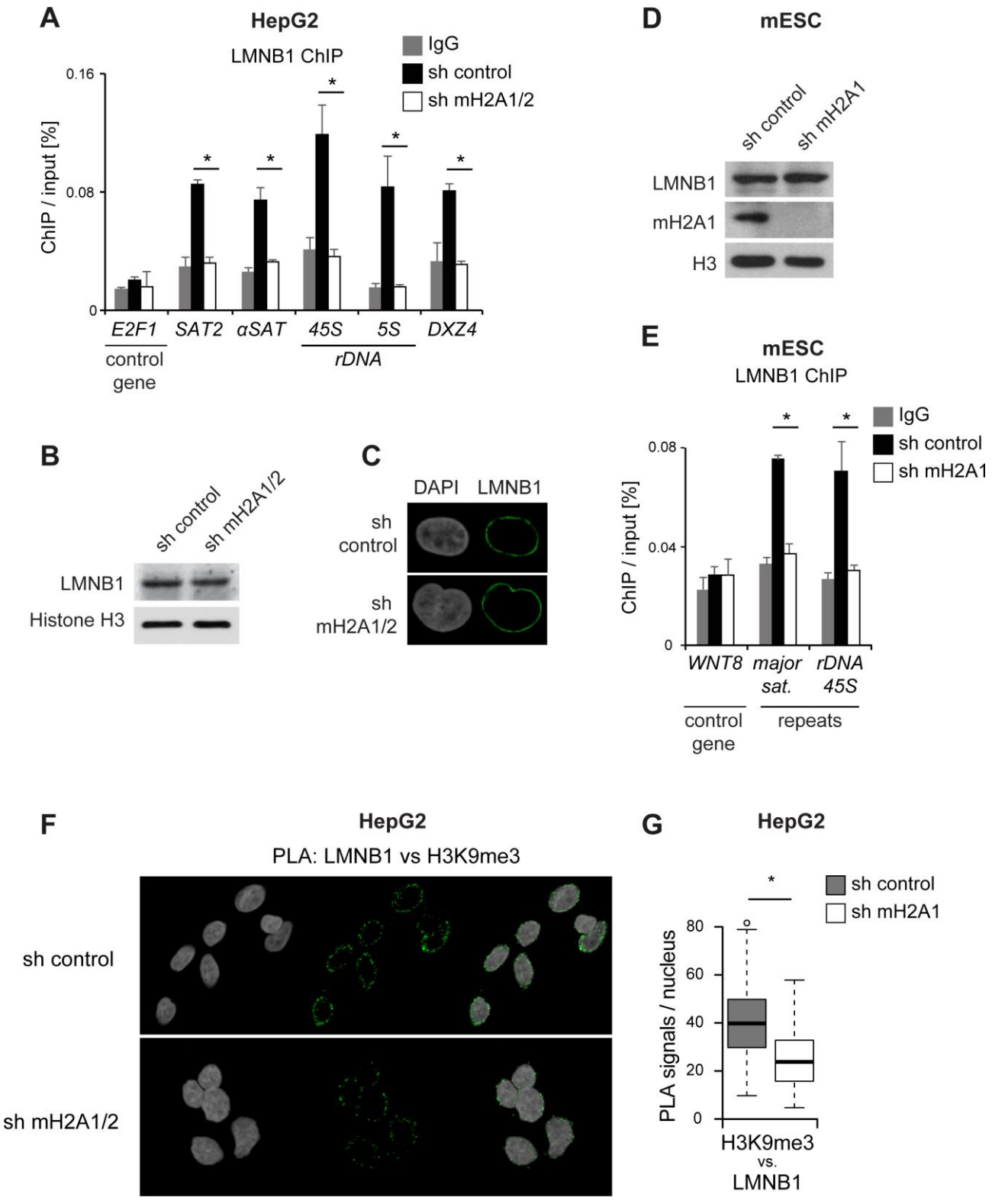

Figure 6. MacroH2A is essential for interaction of Lamin B1 with repeats.

(A) LaminB1 (LMNB1) occupancy on repeats was analyzed by ChIP-qPCR in sh control and sh mH2A1/2 HepG2 cells. Data is represented as mean + s.e.m. (n=3). Student's 2-tailed t-test was used to compare the two groups; *, $p < 0.05$.

(B) LMNB1 immunostaining in HepG2 sh control and sh macroH2A1/2 (mH2A1/2) double knockdown cells. DNA was counterstained with DAPI.

(C) Western blot analysis of LaminB1 and histone H3 in the same cells.

(D) Western blot analysis of macroH2A1, LMNB1 and histone H3 in mouse embryonic stem cells (ESC) cells stably expressing control sh RNA or sh mH2A1.

(E) LMNB1 occupancy on repeats was analyzed by ChIP-qPCR in the ESCs shown in (A). Data is represented as mean + s.e.m. (n=3). Student's 2-tailed t-test was used to compare the two groups; *, $p < 0.05$.

(F) Detection of LMNB1 – H3K9me3 interaction by PLA in control HepG2 cells and sh mH2A1/2 cells. Cells were counterstained with DAPI.

(G) Quantification of detected PLA signals per nucleus in the images obtained in (F). Wilcoxon rank sum test was used to compare the control and sh mH2A1/2 groups (n = 97); *, $p < 0.05$.

SUPPLEMENTARY FIGURES

MacroH2A histone variants maintain nuclear organization and heterochromatin architecture

Julien Douet, David Corujo, Roberto Malinverni, Justine Renauld, Viola Sansoni, Melanija P. Marianovic, Neus Cantariño, Vanesa Valero, Fabien Mongelard, Philippe Bouvet, Axel Imhof, Marc Thiry and Marcus Buschbeck

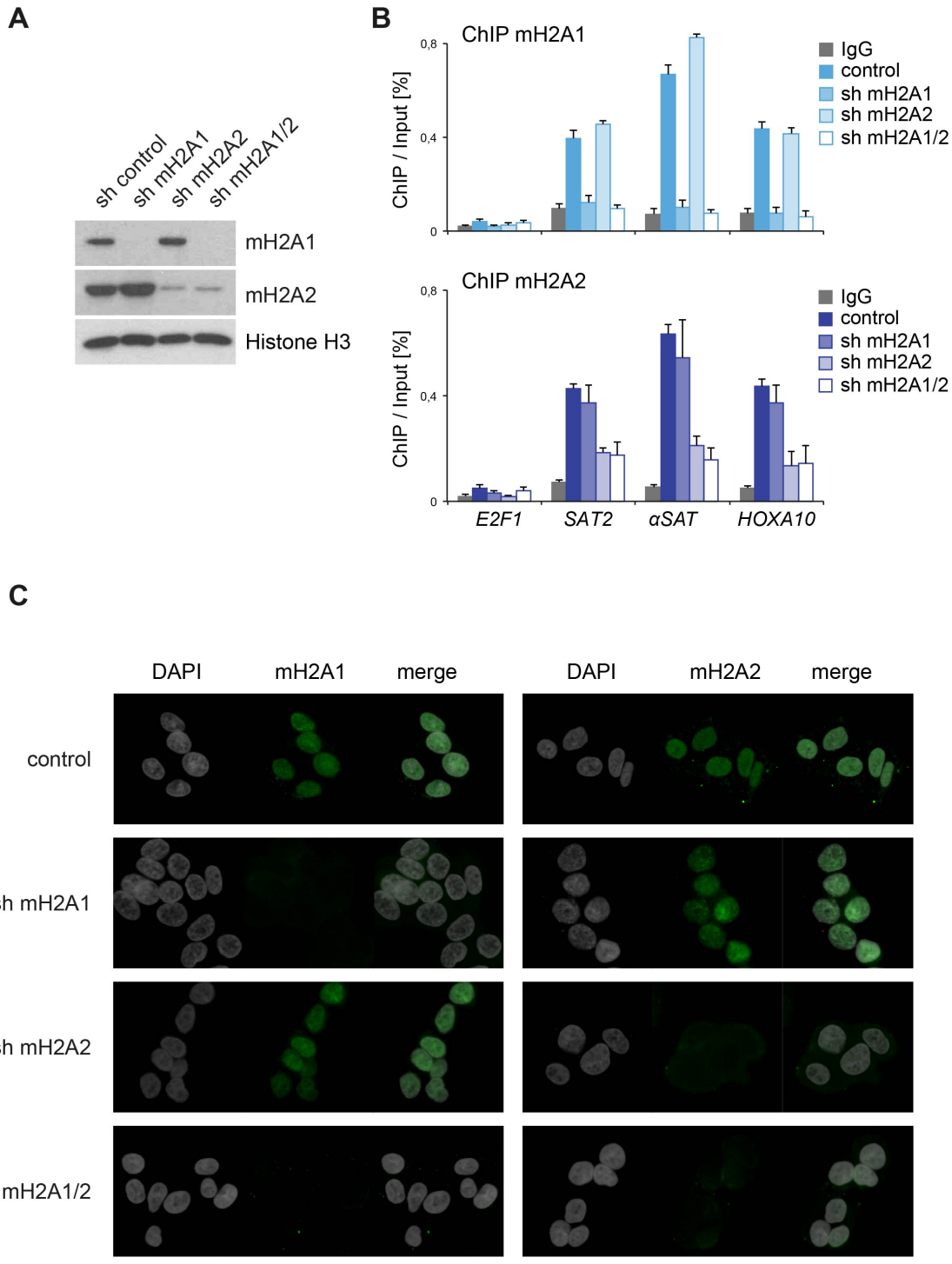

Figure S1. Specificity of macroH2A1 and macroH2A2 antibodies.

(A) Western blot showing the detection of macroH2A1 and macroH2A2 in HepG2 cells depleted for macroH2A1, macroH2A2 or both (sh mH2A1; sh mH2A2; sh mH2A1/2) and control cells (sh control). Immunoblotting of histone H3 has been included to ensure equivalent loading of protein.

(B) Detection of macroH2A1 and macroH2A2 on SAT2 and *αSAT* repeats and *HOXA10* by ChIP in the same cells as in (A). E2F1 was used as included as lowly enriched control locus.

(C) Detection of macroH2A1 and macroH2A2 by immunostaining in the same cells as in (A).

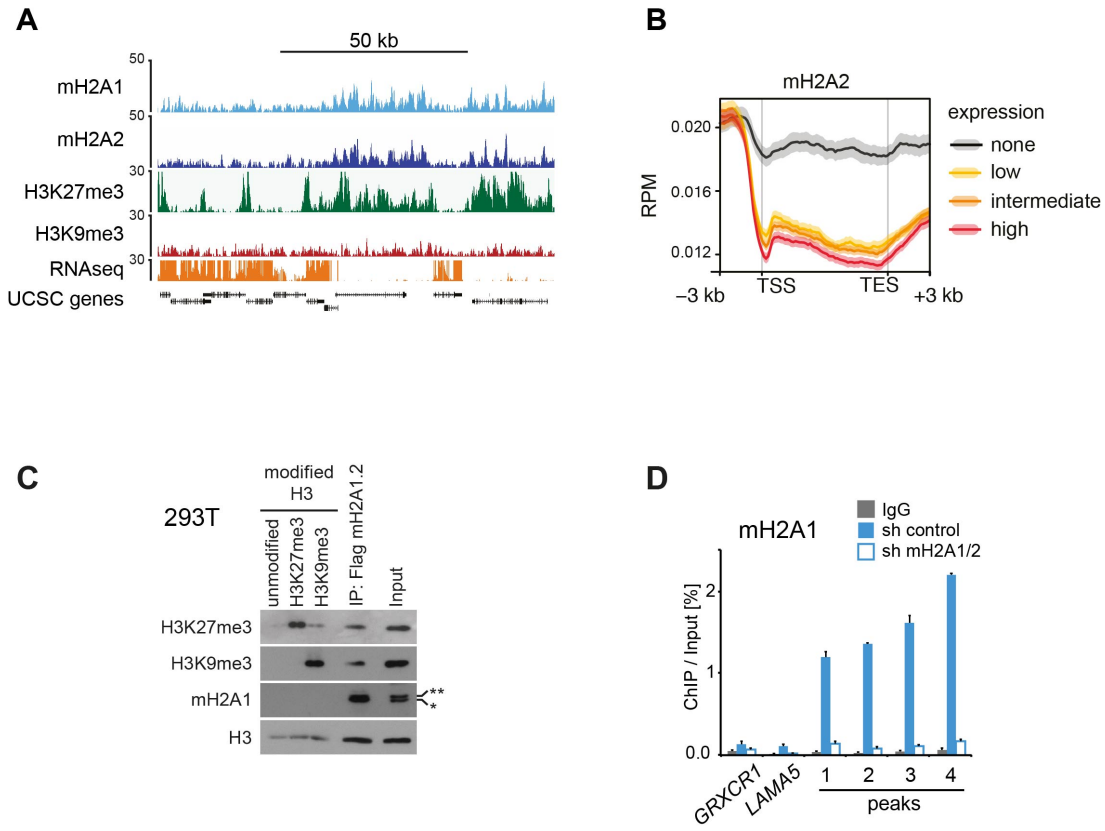

Figure S2. MacroH2A associates with H3K9me3 on interstitial chromatin (related to Figure 2).

(A) Screenshot from the UCSC genome browser showing ChIP-seq profiles of macroH2A1 and macroH2A2 and a RNA-seq track illustrating gene expression. Positions of genes are shown by UCSC genes prediction track.

(B) Normalized read distribution of macroH2A2 on target-genes in HepG2 cells. MacroH2A2 target-genes were divided in 4 categories according to their expression levels: high, intermediate, low expression and none. Please note that average read distribution on gene bodies is plotted after normalization for the size of transcribed regions, while regions upstream of the transcription start site (TSS) and downstream of the transcription end site (TES) are plotted linear. RPM, read count per million.

(C) MacroH2A1.2-containing nucleosomes contain comparable amounts of H3K9me3 and H3K27-marked Histone H3. MacroH2A-containing nucleosomes were anti-FLAG affinity purified from lysates of HEK293T cells stably expressing FLAG-macroH2A1.2 and analyzed by immunoblotting using indicated antibodies. Pure modified histone H3 proteins generated by chemical ligation were used as reference samples.

(D) Occupancy of macroH2A1 at the same positions as in Figure 2E was analyzed by ChIP-qPCR in the same control and knockdown cells. Error bars denote SEM.

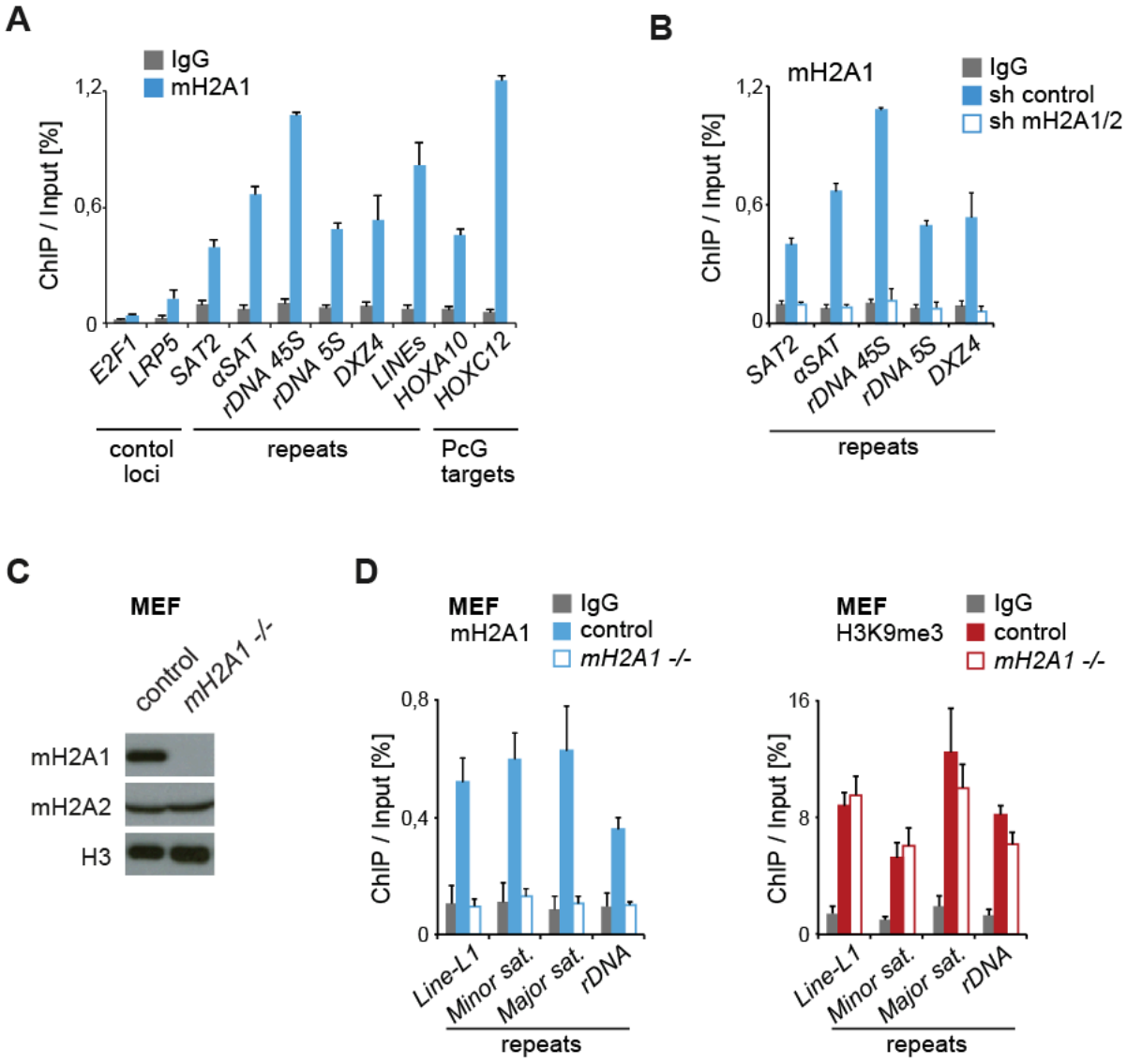

Figure S3. MacroH2A1 occupies repeats of constitutive heterochromatin (related to Figure 3).

(A) Occupancy of macroH2A1 (mH2A1) at the same positions as in Figure 3B was analyzed by ChIP-qPCR in the same control and knockdown cells. Error bars denote SEM.

(B) mH2A1 occupancy on repeats was analyzed by ChIP-qPCR as in Figure 3C. Error bars denote SEM.

(C) Western blot showing the levels of macroH2A1 (mH2A1), macroH2A2 (mH2A2) and histone H3 in control mouse embryonic fibroblasts (MEFs) and *mH2A1* knockout MEFs (*mH2A1* -/-).

(D) macroH2A1 and H3K9me3 occupancy on *Line-L1*, minor satellite (*Minor sat*) and major satellite (*Major sat*) and *rDNA* repeats analysed by ChIP-qPCR in MEF control cells (control) and *mH2A1* knockout cells (mH2A1 -/-). IgG was used as background control. Results were normalized to histone H3 ChIP. Error bars denote SEM.

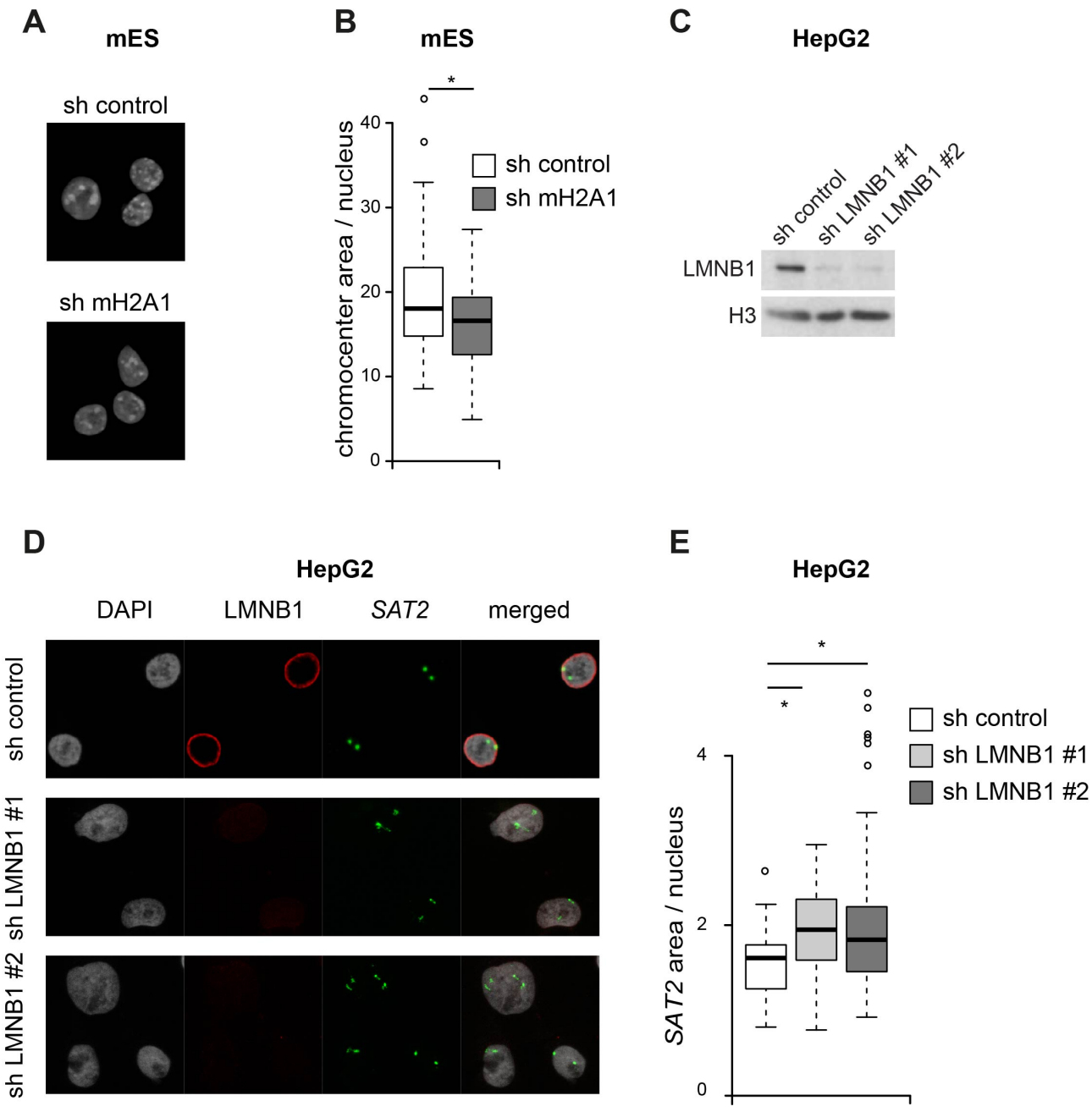

Figure S4. Heterochromatin alterations caused by macroH2A are reminiscent of alterations caused by Lamin B1 knockdown.

(A) DAPI staining of nuclei from control and mH2A1 knockdown mouse embryonic stem (ES) cells.

(B) Percentage of the nuclear area occupied by chromocenters (heterochromatin content) stained by DAPI as shown in (A). Wilcoxon rank sum test was used to compare control (n=68) and knockdown cells (n=56). *, $p < 0.05$.

(C) Western blot analysis of Lamin B1 and histone H3 in HepG2 control cells and two independent shRNA-mediated knockdowns of Lamin B1 (sh LMNB1 #1 and sh LMNB1 #2).

(D) ImmunoFISH detection of LMNB1 (red) and *SAT2* repeats (green) in the same cells. Nuclei were counterstained with DAPI.

(E) Quantification of the fraction of the nucleus occupied by *SAT2* repeats in % of nucleus area (control n=52; sh LMNB1 #1 n=58; sh LMNB1 #2 n=106). Wilcoxon rank sum test was used to compare cells control and sh LMNB1 groups. *, $p< 0.05$.

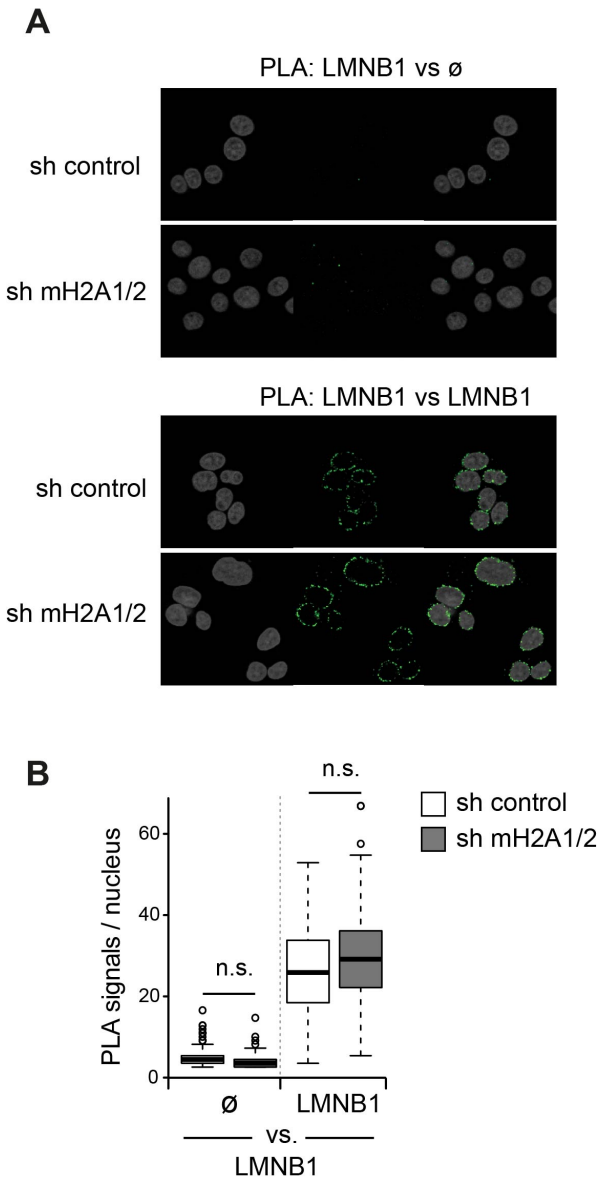

Figure S5. Proximity ligation assay allows to visualize protein interactions.

(A) Detection of Lamin B1 (LMNB1) – Lamin B1 interaction by proximity ligation assay (PLA) using two different antibodies in control HepG2 cells and sh mH2A1/2 cells. PLAs with a single LMNB1 antibody was included as negative control. Cells were counterstained with DAPI.

(B) Quantification of detected PLA signals per nucleus in the images obtained in A; n ≥ 100. Wilcoxon rank sum test was used to compare the control and sh mH2A1/2 groups; n.s., not significant.

SUPPLEMENTARY TABLES

UCSC screenshots	position (hg 19)
peak #1	chr12:29940250-29950695
peak #2	chr1:22900334-22911017
peak #3	chr12:117560996-117571038
peak #4	chr18:37376907-37386906
Region Fig. S1A	chr2:220070682-220178217

Table S1: List of positions shown as UCSC genome browser screenshots.

Application[1]	Primer name	Sequence (5'->3')	References[2]	Species[3]
ChIP	CNTNAP2 Fwd	GGATGGGAGAAACAGTGGGA	(Simon et al., 2012)	Hs
	CNTNAP2 Rev	TAGGCAAGAAGGTGTGGGAG		
ChIP	E2F1 Fwd	GCGTTAAAGCCAATAGGAACC		Hs
	E2F1 Rev	AAAGTCCCGGCCACTTTTAC		
ChIP	GRXCR1 Fwd	CCTCTGGTTTGGACAATGAATAG		Hs
	GRXCR1 Rev	ATGGGGCAAGAAAATGAAAG		
ChIP	LAMA5 Fwd	AGAATGCCCCCACCCTAC		Hs
	LAMA5 Rev	TCCCAAGGTCAGGAGTTCAC		
ChIP	LRP5 Fwd	ATACATGCCTCGGACCTCAG		Hs
	LRP5 Rev	AGCACTGGGACCACTAGAAC		
ChIP	Peak #1 Fwd	GTAGGGCACAATGGGTATGG		Hs
	Peak #1 Rev	GCAGCAAGCGTGTAGAATAGAG		
ChIP	Peak #2 Fwd	GAGTGGGGAACACTAAGCAAG		Hs
	Peak #2 Rev	CCAAAGAAAACGACGGAGAG		
ChIP	Peak #3 Fwd	CAGGCGTGTCTTTAGGATGTAG		Hs
	Peak #3 Rev	TGCCACTGACGTGATGATATG		
ChIP	Peak #4 Fwd	GGCACGAATGTGGTATGTATG		Hs
	Peak #4 Rev	GACACACAGGACACGTCACAC		
RT / FISH	rDNA 45S Fwd	CGACGACCCATTCGAACGTCT	(Cong et al., 2013)	Hs
	rDNA 45S Rev	CTCTCCGGAATCGAACCCTGA		
ChIP	rDNA 45S Fwd	ACCGTGTGGTTTTGGAACCT		Hs
	rDNA 45S Rev	ACCGTGTGGTTTTGGAACCT		
ChIP	rDNA 45S Fwd	GCGCAGCGTTTGCTCTCT		Mm
	rDNA 45S Rev	CACACAAGCCGAGCCACAT		
ChIP/RT	rDNA 5s Fwd	TCTACGGCCATACCACCCTGA	(Shen et al., 2013)	Hs
	rDNA 5s Rev	GCCTACAGCACCCGGTATTCC		
ChIP/RT	DXZ4 Fwd	GCCTACGTCACGCAGGAAG		Hs
	DXZ4 Fwd	TATGTTTGGGCAGGAAGATCG		
ChIP/RT	αSAT_chr4 Fwd	TCATTCCCACAAACTGCGTTG	(Zeng et al., 2009)	Hs
	αSAT_chr4 Rev	TCCAACGAAGGCCACAAGA		
ChIP/RT/FISH	SAT2_chr1 Fwd	CATCGAATGGAAATGAAAGGAGTC	(Zeng et al., 2009)	Hs
	SAT2_chr1 Rev	ACCATTGGATGATTGCAGTCAA		
RT	GAPDH Fwd	GAGTCAACGGATTTGGTCGT		Hs
	GAPDH Rev	TTGATTTTGGAGGGATCTCG		
ChIP	HOXA10 Fwd	GAGGCATCTAGGCGAAAGTG		Hs
	HOXA10 Rev	TTTTTGCCCTCCCACAAC		
ChIP	HOXC12 Fwd	GCGAGCATAATCTCCTGAATC		Hs
	HOXC12 Rev	CTCCCGTGTGGATGTTTACC		
RT	RPO Fwd	TTCATTGTGGGAGCAGAC		Hs/ Mm
	RPO Rev	CAGCAGTTTCTCCAGAGC		
ChIP	MBOAT7 Fwd	CTTCGGAGGTAGTCGAGTCC	(Simon et al., 2012)	Hs
	MBOAT7 Rev	CCTAGCGTCACTTGTACCCA		
ChIP	Major Sat. Fwd	TGGAATATGGCGAGAAAACTG	(Millanes-Romero et al., 2013)	Mm
	Major Sat. Rev	AGGTCCTTCAGTGGGCATTT		
ChIP	Minor Sat. Fwd	GAAAATGATAAAAACCACAC	(Millanes-Romero et al., 2013)	Mm
	Minor Sat. Rev	ACTCATTGATATACACTGTT		
ChIP	Line-L1 Fwd	TTTGGGACACAATGAAAGCA	(Martens et al., 2005)	Mm
	Line-L1 Rev	CTGCCGTCTACTCCTCTTGG		
ChIP	WNT8a Fwd	TGTGTGCATGTGCAATGTATG		Mm
	WNT8a Rev	CACCACTCATACCCACAGAC		

Table S2: List of primers used. [1]Applications: ChIP-PCR (ChIP), RT-qPCR (RT) and Fluorescence in situ hybridization (FISH). [2]References for previously described oligos are given. [3]Species: Human (Hs), Mouse (mm).

References

Cong, R., Das, S., Douet, J., Wong, J., Buschbeck, M., Mongelard, F. and Bouvet, P. (2013). macroH2A1 histone variant represses rDNA transcription. *Nucleic Acids Research* **42**, 181–192.

Martens, J. H., O'Sullivan, R. J., Braunschweig, U., Opravil, S., Radolf, M., Steinlein, P. and Jenuwein, T. (2005). The profile of repeat-associated histone lysine methylation states in the mouse epigenome. *The EMBO Journal* **24**, 800–812.

Millanes-Romero, A., Herranz, N., Perrera, V., Iturbide, A., Loubat-Casanovas, J., Gil, J., Jenuwein, T., de Herreros, A. G. and Peiró, S. (2013). Regulation of Heterochromatin Transcription by Snail1/LOXL2during Epithelial-to-Mesenchymal Transition. *Molecular Cell* **52**, 746–757.

Shen, M., Zhou, T., Xie, W., Ling, T., Zhu, Q., Zong, L., Lyu, G., Gao, Q., Zhang, F. and Tao, W. (2013). The Chromatin Remodeling Factor CSB Recruits Histone Acetyltransferase PCAF to rRNA Gene Promoters in Active State for Transcription Initiation. *PLoS ONE* **8**, e62668.

Simon, J. M., Giresi, P. G., Davis, I. J. and Lieb, J. D. (2012). Using formaldehyde-assisted isolation of regulatory elements (FAIRE) to isolate active regulatory DNA. *Nature Protocols* **7**, 256–267.

Zeng, W., de Greef, J. C., Chen, Y.-Y., Chien, R., Kong, X., Gregson, H. C., Winokur, S. T., Pyle, A., Robertson, K. D., Schmiesing, J. A., et al. (2009). Specific Loss of Histone H3 Lysine 9 Trimethylation and HP1γ/Cohesin Binding at D4Z4 Repeats Is Associated with Facioscapulohumeral Dystrophy (FSHD). *PLoS Genet* **5**, e1000559.